conserved domain from Pfam (http://pfam.sanger.ac.uk/)[51] and predicted intrinsically disordered regions are also displayed. When 3D structure information for the protein is available, the positions of mutation and SNP data can be viewed on the monomer or complex 3D structures with the Jmol applet (Fig. 4B). Detailed information about nucleotide or amino acid residues of interest is displayed in another window after clicking on a residue (Fig. 4C). In particular, at the protein level, an amino acid residue becomes highlighted in the 3D structure when clicking on it (Fig. 4B). The amino acid sequence of human can be compared with those of other organisms by clicking 'Multiple Alignment' button (Fig. 4D). The representation of the 3D structure can be selected from two model types (ribbon or space-filling models) and three colouring types (by rainbow, highlighting mutation positions or residue conservation) (Fig. 4E). The 'External Links' button provides links to NCBI Entrez Gene (http://www.ncbi.nlm.nih.gov/sites/entrez?db=gene)[52] for general information regarding the gene, Human Protein Reference Database (http://www.hprd.org/)[53] for information about the gene product, GeneCards (http://www.genecards.org/),[54] the Reference Database of Immune Cells (http://refdic.rcai.riken.jp/)[55] for gene expression profiling data and the KEGG pathway (http://www.genome.jp/)[56] for pathways involving this gene (Fig. 4F). By using this visualization facility, mapping amino acid positions of known ns substitutions on the crystal structure of the STAT3–DNA complex (PDB code: 1bg1)[57] revealed that the disease-associated missense mutation residue positions were spatially located at the interface of the homodimer or at the DNA binding site, whereas the nsSNP residue positions were located on a surface outside of the molecular interaction sites (Fig. 5). This suggests that disease-causative missense mutations in *STAT3* directly affect the protein–protein and/or protein–DNA interaction as reported previously.[49,50] This is a good demonstration how Mutation@A Glance could help us interpret mutation effects at the molecular level.

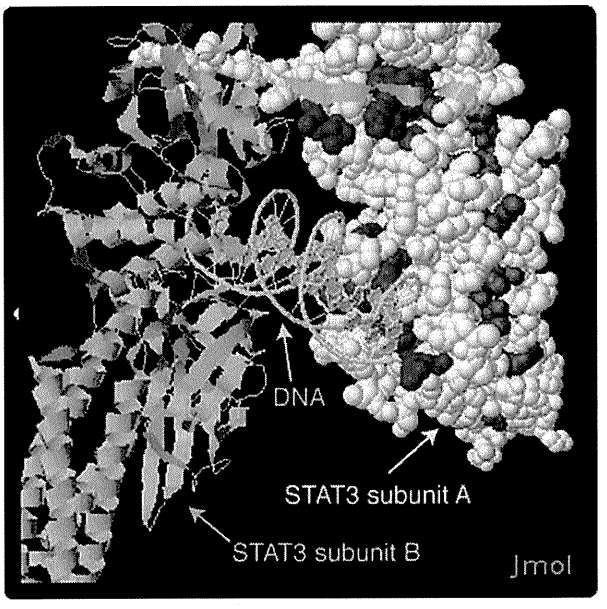

Figure 5. Spatial localization of disease-associated missense mutation sites on the STAT3 protein structure. Two STAT3 subunits are represented as a space-filling model coloured white (subunit A) and a ribbon model coloured pink (subunit B), respectively. A double-stranded DNA is represented as a ribbon model coloured light green. The disease-related missense mutations and nsSNPs of STAT3 (subunit A) are coloured magenta and green, respectively.

3.4. *Evaluating the sequence variations in query sequences*

One of the issues of diagnosis of genetic diseases is how to evaluate the pathogenicity of newly identified sequence variations. To address this issue, Mutation@A Glance has an interface that allows clinical researchers to assess the impact of an observed sequence variation in a given DNA sequence for a candidate disease-causing gene as the second query form (Fig. 3B). When a user submits DNA sequences of a candidate gene in question, this tool returns a list of sequence variations found in the input DNA sequences at both the DNA and the protein levels (Fig. 6). To identify genetic variations that occur in input DNA sequences of a given gene, the BLAT program[58] is implemented to align the input DNA sequences with the reference genomic DNA sequence for the corresponding gene. Figure 6A represents the alignment status of the query sequence to the reference sequence. If a sequence variation is found, multiple lines of detailed information about the variation, such as the variation types (e.g. substitution, insertion and deletion), the mutated region (e.g. exon, intron and 5′- or 3′-splice sites constituting the GT-AG rule), the amino acid changes (e.g. missense, nonsense, insertion/deletion and frame-shift), the known variation data (disease-associated mutation and SNP) and structure/function features of the position at the protein level, are displayed based on the reference human genome sequence in the public database (Fig. 6B). Sequence alignments between the query and reference sequences are also displayed (Fig. 6C). If a ns substitution is found in the query DNA sequence, it was evaluated by the SIFT program[26] (incorporated in the local system), which predicts whether amino acid substitutions in a protein will be 'Deleterious' or 'Tolerated' using evolutionary information from the homologous proteins (Fig. 6B). We tested the prediction accuracy of SIFT with our data sets of disease-associated mutations and non-disease-associated nsSNPs, and found that the

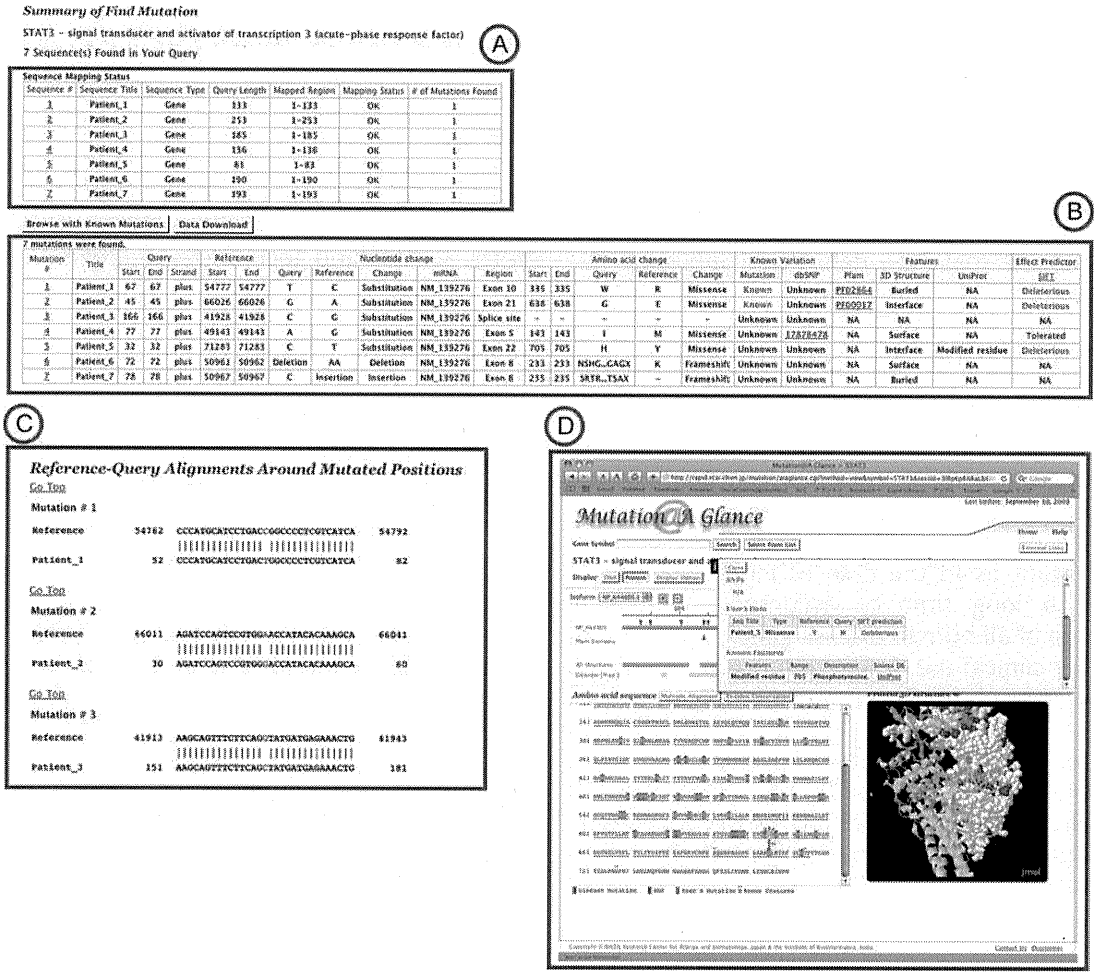

Figure 6. An example of evaluating sequence variations in query *STAT3* DNA sequences. (A) The mapping status of each query sequence to the reference sequence is shown. (B) If a variation is found in the query sequence, the detailed information is shown for each variation (e.g. the positions on the DNA/protein sequences, the type of variation and the description as to whether or not it is known as a disease-associated mutation or SNP). Results from the SIFT program ('Tolerated' or 'Deleterious') are also shown if the variation caused ns substitutions. (C) The query-reference sequence alignment around the altered nucleotides is depicted. (D) The variations can be visualized in the viewer, represented by different colours for known disease mutations or SNPs as 'User's Data'.

false-negative rate (falsely predicted as 'Tolerated' for disease-associated mutations) and the false-positive rate (falsely predicted as 'Deleterious' for nsSNPs) were 25% and 39%, respectively. These accuracy values were comparable to those evaluated in previous study.[33] The current version of Mutation@A Glance does not implement a method for quantitative evaluation of mutation effects on RNA splicing, mainly because we considered the evaluation method is not matured enough yet. However, because the evaluation of mutation effects on RNA splicing/stability is very intriguing, we will place a high priority on the implementation of the evaluation tool for genetic variations affecting RNA splicing/stability in the future development.

There are several advantages of Mutation@A Glance over other existing web servers for evaluating the effects of mutations. First, users are only required to have DNA sequences from a particular gene as their input and thus do not need to pre-process their submission data; other websites for evaluating the mutation effects require a list of genetic variations as a query, not raw sequence data.[26–31] Secondly, Mutation@A Glance identifies and addresses multiple types of sequence variations (e.g. insertion/deletion, frame-shifts) from input query DNA sequences whereas the other web servers do not. Thirdly, newly identified genetic variations can be easily compared with known mutation and SNP data using the graphical visualization interface of Mutation@A Glance (Fig. 6D).

From a viewpoint of clinical use, it is obvious that any mutation analysis platform cannot serve as a useful one without reliable mutation data sets. However, whereas large amounts of disease-associated mutation

data for various genetic diseases have been reported, most of them are dispersed and stored locally. Only a few websites, e.g. OMIM and UniProt, integrate disease-associated mutation data and allow us to download their contents. However, the mutation data in such databases have a relatively low integrity in terms of updating and coverage. Thus, we have begun to comprehensively collect and manually curate the disease-associated mutation data from published literature focusing on PIDs and established a resource of PID research for clinical use, named RAPID.[17] Mutation@A Glance thus uses these manually curated data sets for over 150 PID genes in the RAPID database, which is solid enough for clinical use at least for PID analysis. To make Mutation@A Glance a reliable and general mutation analysis platform for other various genetic diseases in the future, we consider that data sharing with experts in particular diseases will be highly important as in the case of PID; otherwise it would take a long time to accumulate extensive mutation data of all human disease genes to an acceptable level for clinical use. In fact, similar efforts along this direction have been being made by the research community.[19]

As new technologies for determining genetic variation in humans have rapidly and continuously emerged (such as next generation DNA sequencing), amounts of genetic variation data of human are exponentially growing.[6,7,59] Therefore, we will continue to update and improve the Mutation@A Glance system, in order to cope with the larger-scale data analysis for more comprehensive identification of disease-causative candidate genes. Implementing API programs into Mutation@A Glance for query submissions and a retrieval system through command line scripts would be more convenient for this purpose.

In summary, Mutation@A Glance provides a highly integrated bioinformatics tool for mutation analysis not only for facilitating visualization of sequence variation data along with various types of information, including primary and tertiary structures of the gene products, but also for evaluating the effects of novel sequence variations in a query input DNA sequence. This tool works solely on a web browser through Internet and is open to the public. Hence, Mutation@A Glance can be used as a 'one-stop' integrated bioinformatics platform for analysing genotype–phenotype relationships of genetic diseases from molecular as well as clinical perspectives.

Acknowledgements: The authors would like to thank Drs Shigeaki Nonoyama, Kohsuke Imai, Hirokazu Kanegane, Toshio Miyawaki, Koichi Oshima, Fumihiko Ishikawa and Reiko Kikuno-Fukaya for their critical suggestions about this work.

Supplementary Data: Supplementary Data are available at www.dnaresearch.oxfordjournals.org.

Funding

This work is supported by a Grant-in-aid for Special Coordination Funds for Promoting Science and Technology, from the Ministry of Education, Culture, Sports, Science and Technology of Japan.

References

1. Amberger, J., Bocchini, C.A., Scott, A.F. and Hamosh, A. 2009, McKusick's Online Mendelian Inheritance in Man (OMIM), *Nucleic Acids Res.*, **37**, D793–6.
2. Notarangelo, L., Casanova, J.L., Fischer, A., et al. 2004, Primary immunodeficiency diseases: an update, *J. Allergy Clin. Immunol.*, **114**, 677–87.
3. Geha, R.S., Notarangelo, L.D., Casanova, J.L., et al. 2007, Primary immunodeficiency diseases: an update from the International Union of Immunological Societies Primary Immunodeficiency Diseases Classification Committee, *J. Allergy Clin. Immunol.*, **120**, 776–94.
4. Notarangelo, L.D. and Sorensen, R. 2008, Is it necessary to identify molecular defects in primary immunodeficiency disease?, *J. Allergy Clin. Immunol*, **122**, 1069–73.
5. Frazer, K.A., Ballinger, D.G., Cox, D.R., et al. 2007, A second generation human haplotype map of over 3.1 million SNPs, *Nature*, **449**, 851–61.
6. Kryukov, G.V., Shpunt, A., Stamatoyannopoulos, J.A. and Sunyaev, S.R. 2009, Power of deep, all-exon resequencing for discovery of human trait genes, *Proc. Natl Acad. Sci. USA*, **106**, 3871–6.
7. Chun, S. and Fay, J.C. 2009, Identification of deleterious mutations within three human genomes, *Genome Res.*, **19**, 1553–61.
8. Sunyaev, S., Ramensky, V., Koch, I., Lathe, W. III, Kondrashov, A.S. and Bork, P. 2001, Prediction of deleterious human alleles, *Hum. Mol. Genet.*, **10**, 591–7.
9. Tavtigian, S.V., Byrnes, G.B., Goldgar, D.E. and Thomas, A. 2008, Classification of rare missense substitutions, using risk surfaces, with genetic- and molecular-epidemiology applications, *Hum. Mutat.*, **29**, 1342–54.
10. Tavtigian, S.V., Greenblatt, M.S., Goldgar, D.E. and Boffetta, P. 2008, Assessing pathogenicity: overview of results from the IARC Unclassified Genetic Variants Working Group, *Hum. Mutat.*, **29**, 1261–4.
11. Tavtigian, S.V., Greenblatt, M.S., Lesueur, F. and Byrnes, G.B. 2008, In silico analysis of missense substitutions using sequence-alignment based methods, *Hum. Mutat.*, **29**, 1327–36.
12. Houdayer, C., Dehainault, C., Mattler, C., et al. 2008, Evaluation of in silico splice tools for decision-making in molecular diagnosis, *Hum. Mutat.*, **29**, 975–82.
13. Stenson, P.D., Mort, M., Ball, E.V., et al. 2009, The Human Gene Mutation Database: 2008 update, *Genome Med.*, **1**, 13.

14. Singh, A., Olowoyeye, A., Baenziger, P.H., et al. 2008, MutDB: update on development of tools for the biochemical analysis of genetic variation, *Nucleic Acids Res.*, **36**, D815–9.
15. Mailman, M.D., Feolo, M., Jin, Y., et al. 2007, The NCBI dbGaP database of genotypes and phenotypes, *Nat. Genet.*, **39**, 1181–6.
16. Piirila, H., Valiaho, J. and Vihinen, M. 2006, Immunodeficiency mutation databases (IDbases), *Hum. Mutat.*, **27**, 1200–8.
17. Keerthikumar, S., Raju, R., Kandasamy, K., et al. 2009, RAPID: Resource of Asian Primary Immunodeficiency Diseases, *Nucleic Acids Res.*, **37**, D863–7.
18. Sherry, S.T., Ward, M.H., Kholodov, M., et al. 2001, dbSNP: the NCBI database of genetic variation, *Nucleic Acids Res.*, **29**, 308–11.
19. Kaput, J., Cotton, R.G., Hardman, L., et al. 2009, Planning the human variome project: the Spain report, *Hum. Mutat.*, **30**, 496–510.
20. Lee, P.H. and Shatkay, H. 2008, F-SNP: computationally predicted functional SNPs for disease association studies, *Nucleic Acids Res.*, **36**, D820–4.
21. Yuan, H.Y., Chiou, J.J., Tseng, W.H., et al. 2006, FASTSNP: an always up-to-date and extendable service for SNP function analysis and prioritization, *Nucleic Acids Res.*, **34**, W635–41.
22. Yue, P., Melamud, E. and Moult, J. 2006, SNPs3D: candidate gene and SNP selection for association studies, *BMC Bioinformatics*, **7**, 166.
23. Chelala, C., Khan, A. and Lemoine, N.R. 2009, SNPnexus: a web database for functional annotation of newly discovered and public domain single nucleotide polymorphisms, *Bioinformatics*, **25**, 655–61.
24. Yang, J.O., Hwang, S., Oh, J., Bhak, J. and Sohn, T.K. 2008, An integrated database-pipeline system for studying single nucleotide polymorphisms and diseases, *BMC Bioinformatics*, **9** (Suppl 12), S19.
25. Frezal, J. 1998, Genatlas database, genes and development defects, *C. R. Acad. Sci. III*, **321**, 805–17.
26. Ng, P.C. and Henikoff, S. 2003, SIFT: predicting amino acid changes that affect protein function, *Nucleic Acids Res.*, **31**, 3812–4.
27. Ramensky, V., Bork, P. and Sunyaev, S. 2002, Human non-synonymous SNPs: server and survey, *Nucleic Acids Res.*, **30**, 3894–900.
28. Thomas, P.D., Campbell, M.J., Kejariwal, A., et al. 2003, PANTHER: a library of protein families and subfamilies indexed by function, *Genome Res.*, **13**, 2129–41.
29. Bromberg, Y. and Rost, B. 2007, SNAP: predict effect of non-synonymous polymorphisms on function, *Nucleic Acids Res.*, **35**, 3823–35.
30. Ferrer-Costa, C., Gelpi, J.L., Zamakola, L., Parraga, I., de la Cruz, X. and Orozco, M. 2005, PMUT: a web-based tool for the annotation of pathological mutations on proteins, *Bioinformatics*, **21**, 3176–8.
31. Bao, L., Zhou, M. and Cui, Y. 2005, nsSNPAnalyzer: identifying disease-associated nonsynonymous single nucleotide polymorphisms, *Nucleic Acids Res.*, **33**, W480–2.
32. Thusberg, J. and Vihinen, M. 2009, Pathogenic or not? And if so, then how? Studying the effects of missense mutations using bioinformatics methods, *Hum. Mutat.*, **30**, 703–14.
33. Ng, P.C. and Henikoff, S. 2006, Predicting the effects of amino acid substitutions on protein function, *Annu. Rev. Genomics Hum. Genet.*, **7**, 61–80.
34. Boutet, E., Lieberherr, D., Tognolli, M., Schneider, M. and Bairoch, A. 2007, UniProtKB/Swiss-Prot, *Methods Mol. Biol.*, **406**, 89–112.
35. Altschul, S.F., Gish, W., Miller, W., Myers, E.W. and Lipman, D.J. 1990, Basic local alignment search tool, *J. Mol. Biol.*, **215**, 403–10.
36. Thompson, J.D., Higgins, D.G. and Gibson, T.J. 1994, CLUSTAL W: improving the sensitivity of progressive multiple sequence alignment through sequence weighting, position-specific gap penalties and weight matrix choice, *Nucleic Acids Res.*, **22**, 4673–80.
37. Berman, H.M., Battistuz, T., Bhat, T.N., et al. 2002, The Protein Data Bank, *Acta Crystallogr. D Biol. Crystallogr.*, **58**, 899–907.
38. Marti-Renom, M.A., Stuart, A.C., Fiser, A., Sanchez, R., Melo, F. and Sali, A. 2000, Comparative protein structure modeling of genes and genomes, *Annu. Rev. Biophys. Biomol. Struct.*, **29**, 291–325.
39. Shen, M.Y. and Sali, A. 2006, Statistical potential for assessment and prediction of protein structures, *Protein Sci.*, **15**, 2507–24.
40. Shrake, A. and Rupley, J.A. 1973, Environment and exposure to solvent of protein atoms. Lysozyme and insulin, *J. Mol. Biol.*, **79**, 351–71.
41. Ward, J.J., McGuffin, L.J., Bryson, K., Buxton, B.F. and Jones, D.T. 2004, The DISOPRED server for the prediction of protein disorder, *Bioinformatics*, **20**, 2138–9.
42. Sunyaev, S., Ramensky, V. and Bork, P. 2000, Towards a structural basis of human non-synonymous single nucleotide polymorphisms, *Trends Genet.*, **16**, 198–200.
43. Vitkup, D., Sander, C. and Church, G.M. 2003, The amino-acid mutational spectrum of human genetic disease, *Genome Biol.*, **4**, R72.
44. Wang, Z. and Moult, J. 2001, SNPs, protein structure, and disease, *Hum. Mutat.*, **17**, 263–70.
45. Ferrer-Costa, C., Orozco, M. and de la Cruz, X. 2002, Characterization of disease-associated single amino acid polymorphisms in terms of sequence and structure properties, *J. Mol. Biol.*, **315**, 771–86.
46. Kono, H., Yuasa, T., Nishiue, S. and Yura, K. 2008, coliSNP database server mapping nsSNPs on protein structures, *Nucleic Acids Res.*, **36**, D409–13.
47. Chen, J.W., Romero, P., Uversky, V.N. and Dunker, A.K. 2006, Conservation of intrinsic disorder in protein domains and families: I. A database of conserved predicted disordered regions, *J. Proteome Res.*, **5**, 879–87.
48. Schuster-Bockler, B. and Bateman, A. 2008, Protein interactions in human genetic diseases, *Genome Biol.*, **9**, R9.
49. Holland, S.M., DeLeo, F.R., Elloumi, H.Z., et al. 2007, STAT3 mutations in the hyper-IgE syndrome, *N. Engl. J. Med.*, **357**, 1608–19.
50. Minegishi, Y., Saito, M., Tsuchiya, S., et al. 2007, Dominant-negative mutations in the DNA-binding

domain of STAT3 cause hyper-IgE syndrome, *Nature*, **448**, 1058–62.
51. Finn, R.D., Tate, J., Mistry, J., et al. 2008, The Pfam protein families database, *Nucleic Acids Res.*, **36**, D281–8.
52. Sayers, E.W., Barrett, T., Benson, D.A., et al. 2009, Database resources of the National Center for Biotechnology Information, *Nucleic Acids Res.*, **37**, D5–15.
53. Keshava Prasad, T.S., Goel, R., Kandasamy, K., et al. 2009, Human Protein Reference Database—2009 update, *Nucleic Acids Res.*, **37**, D767–72.
54. Rebhan, M., Chalifa-Caspi, V., Prilusky, J. and Lancet, D. 1998, GeneCards: a novel functional genomics compendium with automated data mining and query reformulation support, *Bioinformatics*, **14**, 656–64.
55. Hijikata, A., Kitamura, H., Kimura, Y., et al. 2007, Construction of an open-access database that integrates cross-reference information from the transcriptome and proteome of immune cells, *Bioinformatics*, **23**, 2934–41.
56. Kanehisa, M. and Goto, S. 2000, KEGG: kyoto encyclopedia of genes and genomes, *Nucleic Acids Res.*, **28**, 27–30.
57. Becker, S., Groner, B. and Muller, C.W. 1998, Three-dimensional structure of the Stat3beta homodimer bound to DNA, *Nature*, **394**, 145–51.
58. Kent, W.J. 2002, BLAT—the BLAST-like alignment tool, *Genome Res.*, **12**, 656–64.
59. Ahn, S.M., Kim, T.H., Lee, S., et al. 2009, The first Korean genome sequence and analysis: full genome sequencing for a socio-ethnic group, *Genome Res.*, **19**, 1622–9.

LETTERS

IκBζ regulates T_H17 development by cooperating with ROR nuclear receptors

Kazuo Okamoto[1,2,3], Yoshiko Iwai[4], Masatsugu Oh-hora[1,2], Masahiro Yamamoto[5], Tomohiro Morio[6], Kazuhiro Aoki[7], Keiichi Ohya[7], Anton M. Jetten[8], Shizuo Akira[9], Tatsushi Muta[10] & Hiroshi Takayanagi[1,2,3]

Interleukin (IL)-17-producing helper T (T_H17) cells are a distinct T-cell subset characterized by its pathological role in autoimmune diseases[1–3]. IL-6 and transforming growth factor-β (TGF-β) induce T_H17 development, in which the orphan nuclear receptors, RORγt and RORα, have an indispensable role[4–6]. However, in the absence of IL-6 and TGF-β, the ectopic expression of RORγt or RORα leads to only a modest IL-17 production[5,7,8]. Here we identify a nuclear IκB family member, IκBζ (encoded by the *Nfkbiz* gene), as a transcription factor required for T_H17 development in mice. The ectopic expression of IκBζ in naive $CD4^+$ T cells together with RORγt or RORα potently induces T_H17 development, even in the absence of IL-6 and TGF-β. Notably, $Nfkbiz^{-/-}$ mice have a defect in T_H17 development and a resistance to experimental autoimmune encephalomyelitis (EAE). The T-cell-intrinsic function of IκBζ was clearly demonstrated by the resistance to EAE of the $Rag2^{-/-}$ mice into which $Nfkbiz^{-/-}$ $CD4^+$ T cells were transferred. In cooperation with RORγt and RORα, IκBζ enhances *Il17a* expression by binding directly to the regulatory region of the *Il17a* gene. This study provides evidence for the transcriptional mechanisms underlying T_H17 development and points to a molecular basis for a novel therapeutic strategy against autoimmune disease.

IκBζ is a nuclear protein homologous to Bcl3, which interacts with the NF-κB subunit via the ankyrin repeat domain (ARD)[9,10]. In macrophages, IκBζ induced by Toll-like receptor (TLR) stimulation is essential for the induction of a subset of secondary response genes, including *Il6* (refs 11, 12). However, the function of IκBζ in other cell types has not been elucidated.

We explored the expression of IκBζ in helper T-cell subsets and found that IκBζ was most highly expressed in T_H17 cells (Fig. 1a). Thus, we evaluated the involvement of IκBζ in EAE, which is a model of T_H17 cell-mediated autoimmune disease[1]. After myelin oligodendrocyte glycoprotein (MOG) immunization, wild-type mice developed severe paralytic symptoms, whereas $Nfkbiz^{-/-}$ mice exhibited almost no neuronal deficit (Fig. 1b). Histopathological analyses showed inflammatory cell infiltration and demyelination in the spinal cord of the wild-type mice, but not the $Nfkbiz^{-/-}$ mice (Fig. 1c). IL-17 production was reduced in the spleen and lymph node cells from immunized $Nfkbiz^{-/-}$ mice, but interferon-γ (IFN-γ) production was normal (Fig. 1d and Supplementary Fig. 1). These results indicate that $Nfkbiz^{-/-}$ mice have a defect in T_H17 development.

IκBζ expression was also detected in dendritic cells (Fig. 1a), which produce the inflammatory cytokines required for T_H17 development[1,13]. To exclude the possibility that impaired T_H17 development in $Nfkbiz^{-/-}$ mice is caused by a defect in dendritic cells, we evaluated inflammatory cytokine expression in dendritic cells. We confirmed normal production of tumour necrosis factor-α (TNF-α) and expression of CD40 and CD86 in $Nfkbiz^{-/-}$ dendritic cells after TLR stimulation (Supplementary Fig. 2 and data not shown). TLR ligand-induced production of IL-6 was partially suppressed in $Nfkbiz^{-/-}$ dendritic cells (Supplementary Fig. 2), but a co-culture of naive $CD4^+$ T cells and dendritic cells indicated that $Nfkbiz^{-/-}$ dendritic cells were able to support T_H17 development normally (Fig. 1e, f). However, T_H17 development from $Nfkbiz^{-/-}$ naive $CD4^+$ T cells was markedly impaired regardless of the origin of the co-cultured dendritic cells (Fig. 1e, f).

To demonstrate the $CD4^+$ T-cell-intrinsic function of IκBζ *in vivo*, we transferred wild-type or $Nfkbiz^{-/-}$ $CD4^+$ T cells into $Rag2^{-/-}$ mice (Supplementary Fig. 3), and immunized them with MOG peptide. The mice transferred with wild-type $CD4^+$ T cells developed severe EAE, whereas the mice transferred with $Nfkbiz^{-/-}$ $CD4^+$ T cells had only minimal symptoms (Fig. 1g, h). We observed no significant difference in proliferation between wild-type and $Nfkbiz^{-/-}$ $CD4^+$ T cells (Supplementary Fig. 4). The frequencies of IFN-γ^-IL-17^+ and IFN-γ^+IL-17^+ T cells, but not IFN-γ^+IL-17^- T cells, were much lower in the mice that received $Nfkbiz^{-/-}$ $CD4^+$ T cells than wild-type $CD4^+$ T cells, even at early time points after MOG immunization (Fig. 1i). Collectively, $Nfkbiz^{-/-}$ $CD4^+$ T cells have an intrinsic defect in their ability to differentiate into T_H17 cells, resulting in a low sensitivity to EAE.

When activated with anti-CD3 and anti-CD28 under T_H1- and T_H2-polarizing conditions, $Nfkbiz^{-/-}$ naive $CD4^+$ T cells normally produced IFN-γ and IL-4, respectively (Fig. 2a). On activation by the combination of IL-6 and TGF-β (the T_H17-polarizing conditions), IL-17 production in $Nfkbiz^{-/-}$ T cells was significantly reduced compared with wild-type T cells, even when we added IL-23, IL-1α, TNF-α or replaced IL-6 with IL-21 (Fig. 2a, b). The expression of *Il17f*, *Il21*, *Il23r* and *Il22* messenger RNA was much lower in $Nfkbiz^{-/-}$ T cells than in wild-type T cells (Fig. 2c). The expression of *Rorc* (encoding RORγ) and *Rora* (encoding RORα) mRNA was comparable between wild-type and $Nfkbiz^{-/-}$ T cells (Fig. 2d). The mRNA expression of *Runx1*, the aryl hydrocarbon receptor (*Ahr*), *Irf4*, *Socs3* and *Batf*,

[1]Department of Cell Signaling, Graduate School of Medical and Dental Sciences, Tokyo Medical and Dental University, [2]Global Center of Excellence (GCOE) Program, International Research Center for Molecular Science in Tooth and Bone Diseases, [3]Japan Science and Technology Agency (JST), ERATO, Takayanagi Osteonetwork Project, Yushima 1-5-45, Bunkyo-ku, Tokyo 113-8549, Japan. [4]Medical Top Track Program, Medical Research Institute, Tokyo Medical and Dental University, Yushima 1-5-45, Bunkyo-ku, Tokyo 113-8510, Japan. [5]Laboratory of Immune Regulation, Department of Microbiology and Immunology, Graduate School of Medicine, and WPI Immunology Frontier Research Center, Osaka University, 2-2, Yamada-oka, Suita, Osaka 565-0871, Japan. [6]Department of Pediatrics and Developmental Biology, Graduate School of Medical and Dental Sciences, Tokyo Medical and Dental University, Yushima 1-5-45, Bunkyo-ku, Tokyo 113-8519, Japan. [7]Department of Hard Tissue Engineering (Pharmacology), Graduate School of Medical and Dental Sciences, Tokyo Medical and Dental University, Yushima 1-5-45, Bunkyo-ku, Tokyo 113-8549, Japan. [8]Cell Biology Section, Division of Intramural Research, National Institute of Environmental Health Sciences, National Institutes of Health, 111 T.W. Alexander Drive Research Triangle Park, North Carolina 27709, USA. [9]Laboratory of Host Defense, WPI Immunology Frontier Research Center, Osaka University, Yamada-oka 3-1, Suita, Osaka 565-0871, Japan. [10]Laboratory of Cell Recognition and Response, Graduate School of Life Sciences, Tohoku University, Aoba 6-3, Aramaki, Aoba-ku, Sendai 980-8578, Japan.

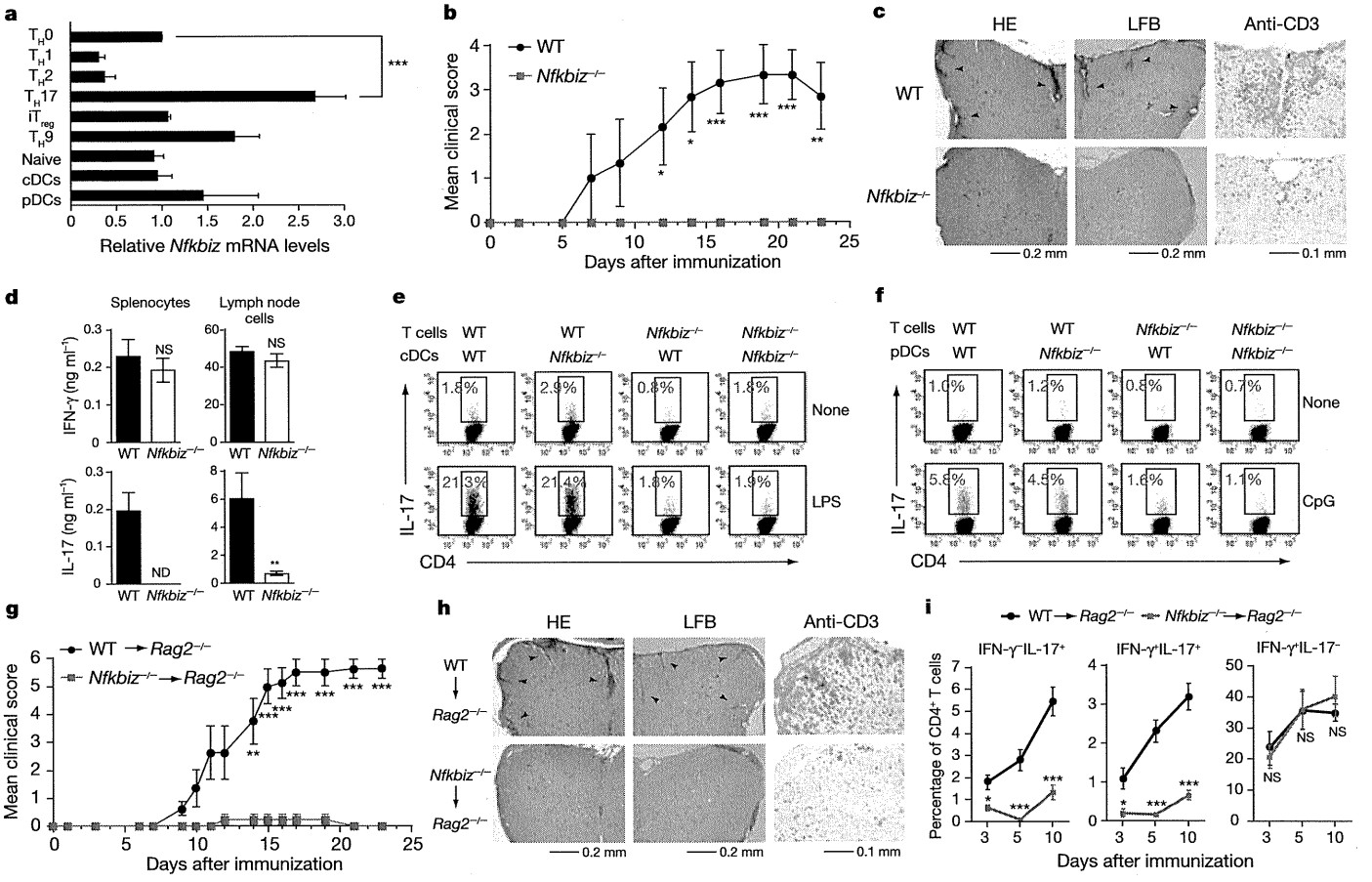

Figure 1 | *Nfkbiz*$^{-/-}$ mice are resistant to EAE owing to a CD4$^+$ T-cell-intrinsic defect in T_H17 development. a, *Nfkbiz* mRNA expression in T_H-cell subsets, inducible T_{reg} (iT_{reg}) cells, naive CD4$^+$ T cells (Naive), conventional dendritic cells (cDCs) and plasmacytoid DCs (pDCs). **b**, Disease course of EAE in wild-type (WT; $n = 5$) or *Nfkbiz*$^{-/-}$ mice ($n = 5$). **c**, Pathology analysis of the spinal cord sections. Arrowheads indicate inflammatory cellular infiltrate (haematoxylin and eosin, HE) and demyelinated areas (Luxol fast blue, LFB). **d**, IFN-γ and IL-17 production in splenocytes and lymph node cells after restimulation with MOG peptide. ND, not detected. **e**, **f**, TLR-induced IL-17 production in CD4$^+$ T cells in co-culture with cDCs (**e**) or pDCs (**f**) isolated from WT or *Nfkbiz*$^{-/-}$ mice. **g**, Disease course of EAE in *Rag2*$^{-/-}$ mice reconstituted with WT ($n = 8$) or *Nfkbiz*$^{-/-}$ ($n = 5$) CD4$^+$ T cells. **h**, Pathology analysis of the spinal cord sections from the reconstituted mice. **i**, Frequency of IFN-γ$^+$IL-17$^+$, IFN-γ$^-$IL-17$^+$ and IFN-γ$^+$IL-17$^-$ CD4$^+$ T cells in the reconstituted mice. Error bars (**a**, **b**, **d**, **g** and **i**), mean ± s.e.m.; $*P < 0.05$; $**P < 0.01$; $***P < 0.005$; NS, not significant.

which are related to T_H17 development[7,14–18], was normal in *Nfkbiz*$^{-/-}$ T cells (Supplementary Fig. 5). The expression of genes related to the migration of T_H17 cells (*Ccr6*, *Ccl20* and *S1pr1*)[2,3] and T_H17-related cytokine receptors (*Il6ra*, *Il6st*, *Il21r*, *Il2rg*, *Il1r1* and *Il1rap*), and IL-6-induced STAT3 phosphorylation, were also normal in *Nfkbiz*$^{-/-}$ T cells (Supplementary Figs 5 and 6). There was no defect in the generation of CD4$^+$CD25$^+$Foxp3$^+$ natural regulatory T (T_{reg}) cells in *Nfkbiz*$^{-/-}$ mice or the *in vitro* development of Foxp3-expressing T_{reg} cells from *Nfkbiz*$^{-/-}$ naive CD4$^+$ T cells (Supplementary Fig. 7). Taken together, IκBζ actively contributes to T_H17 development without affecting T_{reg} cell development.

IκBζ has three alternative splicing variants[10]: IκBζ (L) is the major splicing variant in macrophages, and IκBζ (S) lacks the amino-terminal 99 amino acids of IκBζ (L). Unlike these two variants, the minor splicing variant IκBζ (D) lacks transactivation activity[19]. Immunoblot and PCR with reverse transcription (RT–PCR) analyses showed that T_H17 cells predominantly expressed IκBζ (L) and slightly IκBζ (S), but not IκBζ (D) (Fig. 2e and Supplementary Figs 8 and 9).

IκBζ expression was upregulated by the combination of IL-6 and TGF-β, whereas IL-6 or TGF-β alone had no effect (Fig. 2f and Supplementary Figs 8 and 9). Addition of IL-23 did not have any effect on IκBζ expression (Fig. 2f and Supplementary Fig. 9b). IκBζ expression is regulated by the MyD88-mediated pathway in macrophages[11], and its mRNA is stabilized by the IL-17R-mediated signal in fibroblasts[20]. However, IκBζ is normally induced by the combination of IL-6 and TGF-β in *Myd88*$^{-/-}$ CD4$^+$ T cells, as well as in *Il17a*$^{-/-}$ CD4$^+$ T cells (Fig. 2g and Supplementary Fig. 9d). Notably, IκBζ induction was normal in *Rorc*$^{-/-}$ CD4$^+$ T cells, but severely impaired in Stat3-deficient CD4$^+$ T cells during T_H17 development (Fig. 2g and Supplementary Fig. 9d). Therefore, IκBζ induction is mediated by Stat3, but not by RORγt, in T_H17 cells.

We next investigated the mechanism by which IκBζ regulates T_H17 development. Overexpression of IκBζ in CD4$^+$ T cells induced T_H17 development only when stimulated with IL-6 and TGF-β (Fig. 3a, b and Supplementary Fig. 10), indicating that IκBζ does not act alone, but rather, cooperates with other factor(s) in T_H17 development. Among the T_H17-related cytokines, *Il22* expression was not upregulated by the overexpression of IκBζ without the addition of IL-23 (data not shown). We next determined which domain is responsible for IκBζ function in T_H17 development using IκBζ variants and deletion mutants[19] (Fig. 3c). IκBζ (L) and IκBζ (S) augmented T_H17 development significantly (Fig. 3d), but this augmentation was abolished in IκBζ (D) and IκBζ (L) 457–728, both of which lack the transcriptional activation domain (TAD), as well as in IκBζ (L) 1–456, which lacks the ARD (Fig. 3d). These results indicate that the function of IκBζ in T_H17 cells is dependent on both its transcriptional activity and ARD-mediated interaction with NF-κB.

The interaction between NF-κB p50 (encoded by the *Nfkb1* gene) and IκBζ is necessary for TLR-mediated induction of the inflammatory genes in macrophages[11]. This led us to examine whether p50 is required for IκBζ-mediated T_H17 development. p50 and RelA, but not cRel,

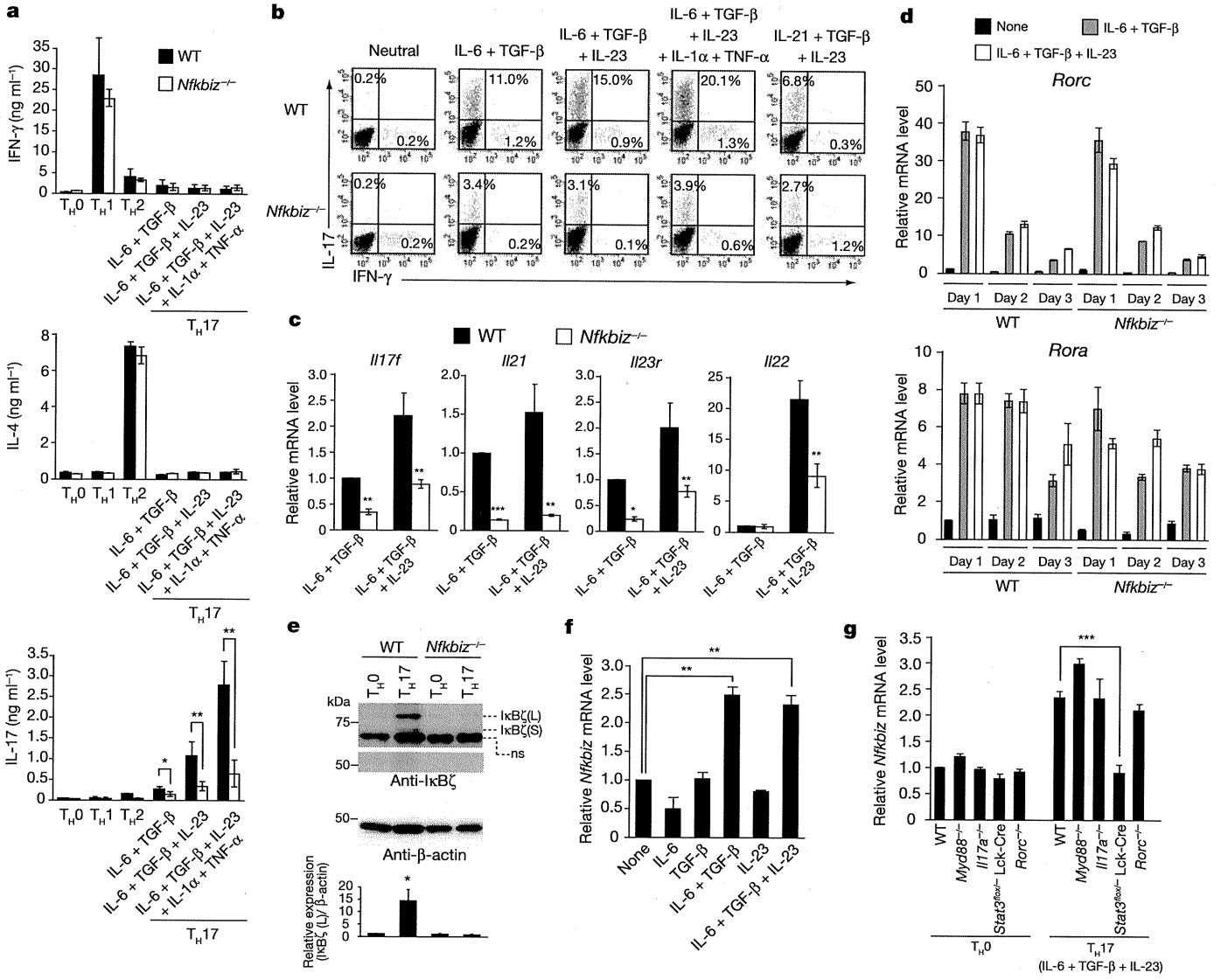

Figure 2 | Targeted disruption of the *Nfkbiz* gene results in impaired T_H17 development. **a**, IFN-γ, IL-4 and IL-17 production in WT or *Nfkbiz*$^{-/-}$ $CD4^+$ T cells activated under T_H0-, T_H1-, T_H2- or T_H17-polarizing conditions. **b**, Intracellular expression of IFN-γ and IL-17 in WT or *Nfkbiz*$^{-/-}$ $CD4^+$ T cells activated under T_H0- or T_H17-polarizing conditions. **c**, *Il17f*, *Il21*, *Il23r* and *Il22* mRNA expression in WT or *Nfkbiz*$^{-/-}$ $CD4^+$ T cells. **d**, *Rorc* and *Rora* mRNA expression in WT or *Nfkbiz*$^{-/-}$ $CD4^+$ T cells cultured for 1, 2 or 3 days. **e**, Protein expression level of the IκBζ splicing variants IκBζ (L) (79 kDa), IκBζ (S) (69 kDa) and IκBζ (D) (57 kDa) in T_H0 or T_H17 cells. ns, non-specific band. **f**, Effects of the cytokines on *Nfkbiz* mRNA expression in $CD4^+$ T cells. **g**, *Nfkbiz* mRNA expression in $CD4^+$ T cells derived from *Myd88*$^{-/-}$, *Il17a*$^{-/-}$, *Stat3*$^{flox/-}$ Lck-Cre or *Rorc*$^{-/-}$ mice. Error bars (**a** and **c**–**g**), mean ± s.e.m.; $*P < 0.05$; $**P < 0.01$; $***P < 0.005$.

enhanced the ability of IκBζ to induce IL-17 production under T_H17-polarizing conditions (Supplementary Fig. 11). However, *Nfkb1*$^{-/-}$ naive $CD4^+$ T cells normally differentiated into T_H17 cells (Supplementary Fig. 12), and ectopic expression of IκBζ enhanced T_H17 development even in *Nfkb1*$^{-/-}$ T cells (Supplementary Fig. 13). Therefore, p50 is not essential for IκBζ-mediated regulation of T_H17 development. In the absence of IL-6 and TGF-β, co-expression of IκBζ and an NF-κB subunit did not induce T_H17 development (Supplementary Fig. 11), indicating that a factor(s) other than NF-κB is required for IκBζ-mediated regulation of T_H17 development.

These results prompted us to test whether IκBζ functions in cooperation with RORγt or RORα in T_H17 development. In the absence of IL-6 and TGF-β, neither the ROR nuclear receptors nor IκBζ induced T_H17 development efficiently (Figs 3a and 4a), but when IκBζ (L) or (S) was overexpressed, either RORγt or RORα strongly induced IL-17 production, even in the absence of exogenous polarizing cytokines (Fig. 4a and Supplementary Fig. 14). These findings indicate that the ROR nuclear receptors and IκBζ synergistically promote T_H17 development. Under T_H17-polarizing conditions, RORγt or RORα alone strikingly induced IL-17 production (Fig. 4a), to which IκBζ induced by the combination of IL-6 and TGF-β may contribute (Fig. 2f and Supplementary Figs 8 and 9). IL-17 production induced by RORγt or RORα overexpression was significantly decreased in *Nfkbiz*$^{-/-}$ T cells under T_H17-polarizing conditions (Fig. 4b), the decrease of which was not restored by the addition of exogenous IL-21 or IL-9 (Supplementary Fig. 15). IL-17 induction was severely impaired when IκBζ was overexpressed in *Rorc*$^{-/-}$ or homozygous *Staggerer* mutation (*Rora*$^{sg/sg}$) cells[21] (Fig. 4c and Supplementary Fig. 16). Taken together, the cooperation of IκBζ with RORγt or RORα is clearly essential for T_H17 development.

Does IκBζ directly regulate the *Il17a* promoter? Seven IκBζ response elements[22] were found within the 6.6-kilobase-pair promoter region of the mouse *Il17a* gene (Fig. 4d). The reporter assay showed that IκBζ (L) and (S) moderately activated the *Il17a* promoter as well as RORγt and RORα (Fig. 4e). When RORγt or RORα was expressed, IκBζ (L) and (S), but not (D), activated the *Il17a* promoter to a much larger extent (Fig. 4e). An evolutionarily conserved non-coding sequences (CNS) 2 region in the *Il17a* locus was reported to be associated with histone H3 acetylation in a T_H17 lineage-specific

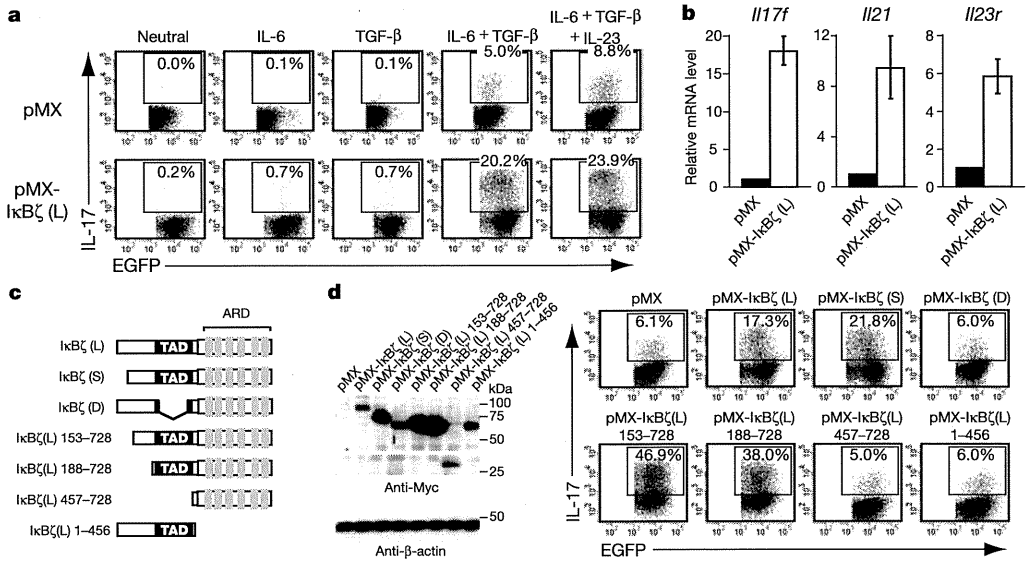

Figure 3 | Ectopic expression of IκBζ facilitates T_H17 development. **a**, Effects of retroviral expression of IκBζ (L) on IL-17 production. **b**, Effects of retroviral expression of IκBζ (L) on *Il17f*, *Il21* and *Il23r* mRNA expression in $CD4^+$ T cells activated in the presence of IL-6 and TGF-β. Error bars, mean ± s.e.m. **c**, Schematic of IκBζ variants and truncated mutants of IκBζ (L). **d**, Effects of retroviral expression of the Myc-tagged IκBζ variants and mutants on T_H17 development (right). Immunoblot analysis of IκBζ protein levels in Myc-tagged IκBζ variants-expressing $CD4^+$ T cells (left). IκBζ (L) 153–728 and IκBζ (L) 188–728 had a more potent activity to induce IL-17 production than IκBζ (L), which may be correlated to their high expression levels.

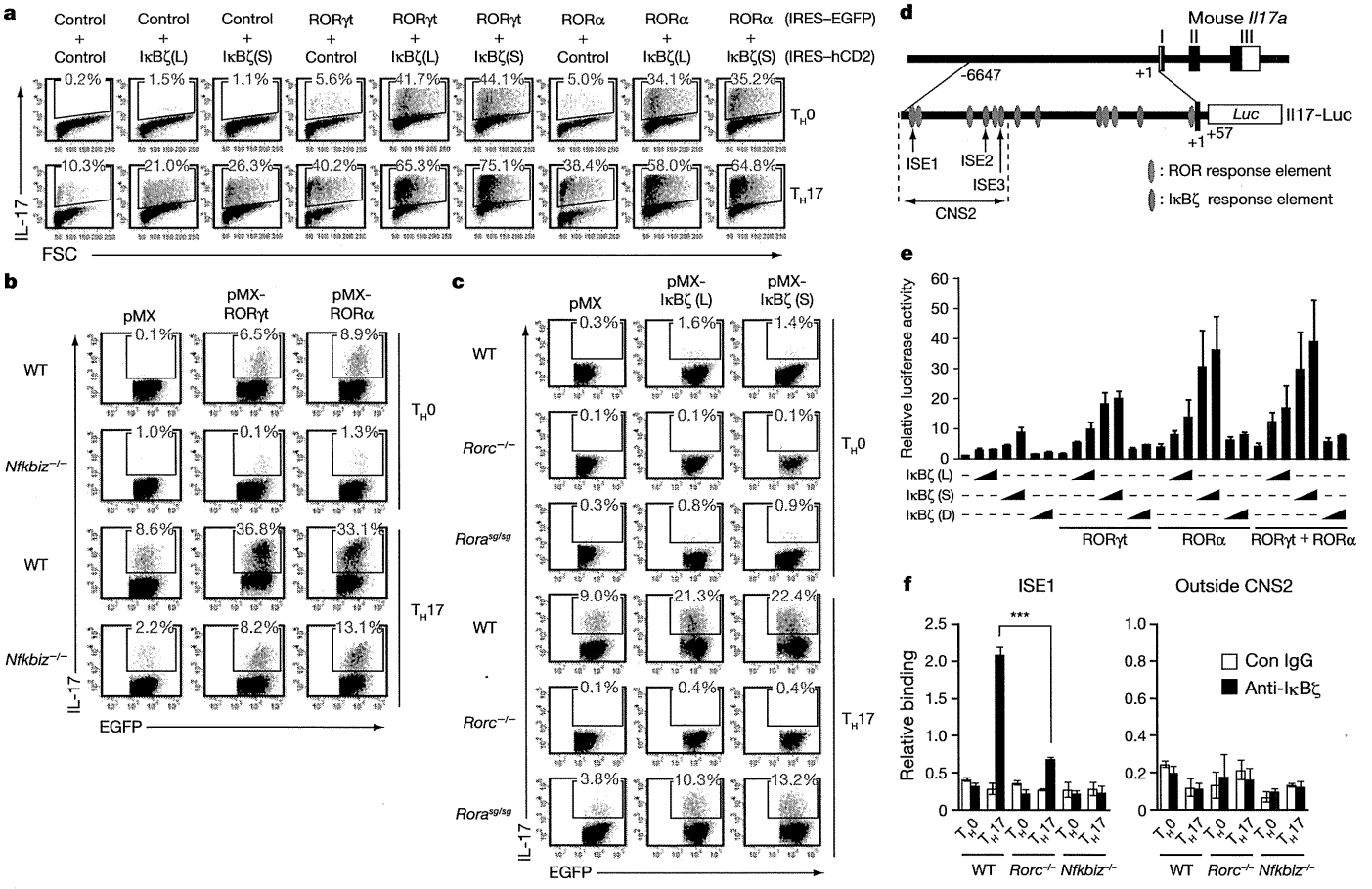

Figure 4 | IκBζ and ROR nuclear receptors cooperatively activate the *Il17a* promoter and facilitate T_H17 development. **a**, IL-17 production in $CD4^+$ T cells transduced with IκBζ (IRES–hCD2) and RORγt or RORα (IRES–EGFP) after activation under T_H0- or T_H17-polarizing conditions. FSC, forward scatter. **b**, Effects of retroviral expression of RORγt or RORα on IL-17 production in WT or *Nfkbiz*$^{-/-}$ $CD4^+$ T cells. **c**, Effects of retroviral expression of IκBζ on IL-17 production in WT, *Rorc*$^{-/-}$ or *Rora*$^{sg/sg}$ $CD4^+$ T cells. **d**, Putative IκBζ and ROR response elements[5,17,21] in the mouse *Il17a* promoter and the Il17-Luc construct. Three IκBζ response elements were located in the CNS2 region (ISE1, −6350 to −6339; ISE2, −4795 to −4786; ISE3, −4454 to −4445). The transcriptional initiation site was designated as +1. **e**, Effects of IκBζ on RORγt and/or RORα-mediated activation of the *Il17a* promoter. **f**, Recruitment of IκBζ to the ISE1 region or the region outside CNS2 (−3978 to −3969) in WT, *Rorc*$^{-/-}$, *Nfkbiz*$^{-/-}$ $CD4^+$ T cells. Error bars (**e** and **f**), mean ± s.e.m. ***$P < 0.005$.

manner and with ROR nuclear receptor-directed IL-17 production[5,17,23]. IκBζ facilitated the CNS2 enhancer activity in combination with RORγt and RORα (Supplementary Fig. 17a, b). However, the *Il17a* promoter region lacking the CNS2 region was not activated by the co-expression of IκBζ and RORγt or RORα (Supplementary Fig. 17a, c, d). IκBζ induced the CNS2 enhancer activity mainly through the distal IκBζ response element (ISE1: −6350 to −6339) (Fig. 4d) among the three IκBζ response elements in the CNS2 region (Supplementary Fig. 18). Chromatin immunoprecipitation (ChIP) experiments showed that IκBζ was recruited to the ISE1 region in T_H17 cells, but not in T_H0 cells (Fig. 4f). We observed no physical interaction between IκBζ and RORγt or RORα by immunoprecipitation assay (data not shown), but recruitment of IκBζ to the ISE1 region was dependent on RORγt (Fig. 4f). These results indicate that T_H17 development entails IκBζ recruitment to the regulatory region of the *Il17a* gene, a process in which ROR nuclear receptors have a critical role.

This study demonstrates that IκBζ, which has a key role in the innate immune response, regulates T_H17 development in a T-cell-intrinsic manner. IκBζ, like Runx1 and Batf[14,17], does not act alone, but in cooperation with ROR nuclear receptors. This does not reduce the importance of IκBζ as the therapeutic target, because disruption of IκBζ alone leads to a complete resistance to EAE (Fig. 1). Runx1, Batf and IRF4 function upstream of RORγt[7,14,17], but it is unlikely that ROR nuclear receptors function downstream of IκBζ or vice versa (Fig. 2d, g and Supplementary Fig. 9d). We speculate that the binding of both IκBζ and ROR nuclear receptors to the *Il17* promoter leads to an efficient recruitment of transcriptional coactivators with histone acetylase activity[5,23]. Moreover, RORγt may be involved in the regulation of the accessibility of IκBζ to the specific transcriptional regulatory regions (Fig. 4f). Interestingly, *Il17f*, *Il21* and *Il23r* mRNA expression was impaired in *Nfkbiz*$^{-/-}$ T cells (Fig. 2c). ChIP analyses showed recruitment of IκBζ to the promoter or the enhancer region of these T_H17-related cytokine genes (Supplementary Fig. 19), indicating that IκBζ directly regulates these genes. *Nfkbiz*$^{-/-}$ mice develop atopic dermatitis-like skin lesions[11,24]. However, as the dermatitis was not observed in the *Rag2*$^{-/-}$ mice reconstituted with *Nfkbiz*$^{-/-}$ $CD4^+$ T cells or *Nfkbiz*$^{-/-}$ fetal liver cells (data not shown), it is not likely that the dermatitis was caused by T-cell-intrinsic abnormalities, including impaired T_H17 development. Thus, the present study demonstrates the T-cell-specific function of IκBζ, which is important for understanding the transcriptional program in T_H17 cell lineage commitment.

METHODS SUMMARY

T-cell differentiation *in vitro*. Naive $CD4^+$ T cells were purified from spleen using the $CD4^+CD62L^+$ T Cell Isolation Kit (Miltenyi Biotec) (purity was >95%) and activated with plate-bound 2 μg ml^{-1} anti-CD3 (145-2C11, BD Biosciences) and 2 μg ml^{-1} anti-CD28 (37.51, BD Biosciences) for 3 days under various polarizing conditions (see Methods for details).

Full Methods and any associated references are available in the online version of the paper at www.nature.com/nature.

Received 12 August 2009; accepted 10 February 2010.
Published online 11 April 2010.

1. Korn, T., Bettelli, E., Oukka, M. & Kuchroo, V. K. IL-17 and Th17 cells. *Annu. Rev. Immunol.* **27**, 485–517 (2009).
2. Dong, C. T_H17 cells in development: an updated view of their molecular identity and genetic programming. *Nature Rev. Immunol.* **8**, 337–348 (2008).
3. O'Shea, J. J. *et al.* Signal transduction and Th17 cell differentiation. *Microbes Infect.* **11**, 599–611 (2009).
4. Ivanov, I. I. *et al.* The orphan nuclear receptor RORγt directs the differentiation program of proinflammatory IL-17$^+$ T helper cells. *Cell* **126**, 1121–1133 (2006).
5. Yang, X. O. *et al.* T helper 17 lineage differentiation is programmed by orphan nuclear receptors RORα and RORγ. *Immunity* **28**, 29–39 (2008).
6. Manel, N., Unutmaz, D. & Littman, D. R. The differentiation of human T_H-17 cells requires transforming growth factor-β and induction of the nuclear receptor RORγt. *Nature Immunol.* **9**, 641–649 (2008).
7. Brüstle, A. *et al.* The development of inflammatory T_H-17 cells requires interferon-regulatory factor 4. *Nature Immunol.* **8**, 958–966 (2007).
8. Huber, M. *et al.* IRF4 is essential for IL-21-mediated induction, amplification, and stabilization of the Th17 phenotype. *Proc. Natl Acad. Sci. USA* **105**, 20846–20851 (2008).
9. Yamazaki, S., Muta, T. & Takeshige, K. A novel IκB protein, IκB-ζ, induced by proinflammatory stimuli, negatively regulates nuclear factor-κB in the nuclei. *J. Biol. Chem.* **276**, 27657–27662 (2001).
10. Muta, T. IκB-ζ: an inducible regulator of nuclear factor-κB. *Vitam. Horm.* **74**, 301–316 (2006).
11. Yamamoto, M. *et al.* Regulation of Toll/IL-1-receptor-mediated gene expression by the inducible nuclear protein IκBζ. *Nature* **430**, 218–222 (2004).
12. Yamamoto, M. & Takeda, K. Role of nuclear IκB proteins in the regulation of host immune responses. *J. Infect. Chemother.* **14**, 265–269 (2008).
13. Veldhoen, M., Hocking, R. J., Atkins, C. J., Locksley, R. M. & Stockinger, B. TGFβ in the context of an inflammatory cytokine milieu supports de novo differentiation of IL-17-producing T cells. *Immunity* **24**, 179–189 (2006).
14. Schraml, B. U. *et al.* The AP-1 transcription factor Batf controls T_H17 differentiation. *Nature* **460**, 405–409 (2009).
15. Quintana, F. J. *et al.* Control of T_{reg} and T_H17 cell differentiation by the aryl hydrocarbon receptor. *Nature* **453**, 65–71 (2008).
16. Veldhoen, M. *et al.* The aryl hydrocarbon receptor links T_H17-cell-mediated autoimmunity to environmental toxins. *Nature* **453**, 106–109 (2008).
17. Zhang, F., Meng, G. & Strober, W. Interactions among the transcription factors Runx1, RORγt and Foxp3 regulate the differentiation of interleukin 17-producing T cells. *Nature Immunol.* **9**, 1297–1306 (2008).
18. Chen, Z. *et al.* Selective regulatory function of Socs3 in the formation of IL-17-secreting T cells. *Proc. Natl Acad. Sci. USA* **103**, 8137–8142 (2006).
19. Motoyama, M., Yamazaki, S., Eto-Kimura, A., Takeshige, K. & Muta, T. Positive and negative regulation of nuclear factor-κB-mediated transcription by IκB-ζ, an inducible nuclear protein. *J. Biol. Chem.* **280**, 7444–7451 (2005).
20. Yamazaki, S., Muta, T., Matsuo, S. & Takeshige, K. Stimulus-specific induction of a novel nuclear factor-κB regulator, IκB-ζ, via Toll/interleukin-1 receptor is mediated by mRNA stabilization. *J. Biol. Chem.* **280**, 1678–1687 (2005).
21. Jetten, A. M. & Joo, J. H. Retinoid-related orphan receptors (RORs): roles in cellular differentiation and development. *Adv. Dev. Biol.* **16**, 313–355 (2006).
22. Matsuo, S., Yamazaki, S., Takeshige, K. & Muta, T. Crucial roles of binding sites for NF-κB and C/EBPs in IκB-ζ-mediated transcriptional activation. *Biochem. J.* **405**, 605–615 (2007).
23. Akimzhanov, A. M., Yang, X. O. & Dong, C. Chromatin remodeling of interleukin-17 (IL-17)-IL-17F cytokine gene locus during inflammatory helper T cell differentiation. *J. Biol. Chem.* **282**, 5969–5972 (2007).
24. Shiina, T. *et al.* Targeted disruption of MAIL, a nuclear IκB protein, leads to severe atopic dermatitis-like disease. *J. Biol. Chem.* **279**, 55493–55498 (2004).

Supplementary Information is linked to the online version of the paper at www.nature.com/nature.

Acknowledgements We are grateful to Y. Iwakura and T. Kitamura for providing *Il17a*$^{-/-}$ mice and retrovirus vectors, respectively. We also thank M. Shinohara, T. Negishi-Koga, M. Asagiri, T. Nakashima, N. Komatsu, M. Ohba, Y. Kunisawa, Y. Suzuki, S. Miyakoshi and T. Kunigami for discussion and assistance. This work was supported in part by Grant-in-Aid for Creative Scientific Research from the Japan Society for the Promotion of Science (JSPS), Grant-in-Aid for Challenging Exploratory Research from JSPS, Grant-in-Aid for JSPS Fellows, Grants-in-Aid for GCOE Program from the Ministry of Education, Culture, Sports, Science and Technology of Japan (MEXT), and ERATO, Takayanagi Osteonetwork Project from JST. It was also supported by grants from the Intramural Research Program of the NIEHS (Z01-ES-101586) (to A.M.J.), Takeda Life Science Foundation and Yokoyama Foundation for Clinical Pharmacology and the Ichiro Kanehara Foundation. Ka.O. is supported by JSPS Research Fellowships for Young Scientists.

Author Contributions Ka.O. performed all of the experiments, interpreted the results and prepared the manuscript. Y.I. contributed to dendritic cells experiments and T-cell transfer experiments. M.O. contributed to study design and manuscript preparation. M.Y., A.M.J. and S.A. provided genetically modified mice and advice on data analysis. To.M. provided advice on project planning and data interpretation. K.A. and Ke.O. supported the experiments using *Nfkb1*$^{-/-}$ mice. Ta.M. provided genetically modified mice and the plasmids, and advised on project planning. H.T. directed the project and wrote the manuscript.

Author Information Reprints and permissions information is available at www.nature.com/reprints. The authors declare no competing financial interests. Correspondence and requests for materials should be addressed to H.T. (taka.csi@tmd.ac.jp).

METHODS

Mice. We used *Nfkbiz*$^{-/-}$ mice on a mixed 129Sv-C57BL/6 background at 5 weeks after birth[11] because of the almost complete embryonic lethality of the inbred C57BL/6 genetic background. *Rorc*$^{-/-}$ (ref. 25), *Myd88*$^{-/-}$ (ref. 26), and *Il17a*$^{-/-}$ (ref. 27) mice on a C57BL/6 background were described previously. *Nfkb1*$^{-/-}$ (ref. 28) and *Rora*$^{sg/+}$ (ref. 29) mice on a C57BL/6 background were obtained from The Jackson Laboratory. *Rag2*$^{-/-}$ mice on a C57BL/6 background were purchased from Taconic Farms. For the generation of mice with T-cell-specific disruption of *Stat3*, Lck-Cre transgenic mice (The Jackson Laboratory) were bred with *Stat3*$^{flox/-}$ mice[30]. We used wild-type littermates as controls in all experiments. All of the animals were maintained in a specific pathogen-free environment, and all animal experiments were performed with the approval of the institutional committee.

T-cell differentiation *in vitro*. The conditions for different T_H cell subsets were: 10 μg ml^{-1} anti-IL-4 (11B11, BD Biosciences) and 10 μg ml^{-1} anti-IFN-γ (XMG1.2, BD Biosciences) for T_H0 (neutral conditions); 10 μg ml^{-1} anti-IL-4 and 10 ng ml^{-1} IL-12 (PeproTech) for T_H1; 10 μg ml^{-1} anti-IFN-γ and 10 ng ml^{-1} IL-4 (PeproTech) for T_H2; 10 μg ml^{-1} anti-IL-4, 10 μg ml^{-1} anti-IFN-γ and 2.5 ng ml^{-1} TGF-β (PeproTech) for inducible T_{reg}; 10 μg ml^{-1} anti-IFN-γ, 10 ng ml^{-1} IL-4 and 1 ng ml^{-1} TGF-β for T_H9; 10 μg ml^{-1} anti-IL-4, 10 μg ml^{-1} anti-IFN-γ, 30 ng ml^{-1} IL-6 (PeproTech), 2.5 ng ml^{-1} TGF-β, 50 ng ml^{-1} IL-23 (R&D Systems), 80 ng ml^{-1} IL-21 (R&D Systems), 10 ng ml^{-1} IL-1α (PeproTech), 10 ng ml^{-1} TNF-α (R&D Systems) or a combination of these stimuli for T_H17. Activated cells were restimulated with 40 ng ml^{-1} phorbol-12-myristate-13-acetate (PMA) (Calbiochem) and 0.5 μg ml^{-1} ionomycin (Sigma-Aldrich) in the presence of GolgiPlug (BD Biosciences) for 4 h before intracellular staining, or restimulated with 2 μg ml^{-1} anti-CD3 and 2 μg ml^{-1} anti-CD28 for 3 days before enzyme-linked immunosorbent assay (ELISA). We cultured cells in RPMI 1640 medium (Invitrogen) unless otherwise indicated, or in IMDM medium (Sigma-Aldrich) in Supplementary Figs 8a, c and 9c.

Induction of EAE. The MOG35–55 peptide (MEVGWYRSPFSRVVHLYRNGK) was synthesized by Biologica. For the induction of EAE, we used 5-week-old *Nfkbiz*$^{-/-}$ mice in which no apparent symptoms of dermatitis were observed. Age-matched wild-type and *Nfkbiz*$^{-/-}$ mice were immunized subcutaneously with the MOG peptide (250 μg per mouse) emulsified in complete Freund's adjuvant (CFA) containing 40 ng ml^{-1} *Mycobacterium tuberculosis* H37RA (Difco Laboratories) (day 0). After immunization, the mice were intraperitoneally injected with pertussis toxin (200 ng per mouse, Sigma-Aldrich) on days 0 and 2. On day 23, lymphoid cells were prepared from the spleens and lymph nodes of the immunized mice, and were then stimulated with 25 μg ml^{-1} MOG peptide, or 2 μg ml^{-1} anti-CD3 and 2 μg ml^{-1} anti-CD28 for 48 h, after which IFN-γ and IL-17 production was analysed by ELISA.

For the induction of EAE in the reconstituted *Rag2*$^{-/-}$ mice, MOG peptide (150 μg per mouse) emulsified in CFA was injected on days 0 and 7. Pertussis toxin (400 ng per mouse) was injected on days 1 and 8. On day 3, 5 or 10, splenocytes isolated from the recipients were stimulated with 2 μg ml^{-1} anti-CD3 and 2 μg ml^{-1} anti-CD28 for 24 h. GolgiPlug was added for the final 4 h of culture, and then intracellular IL-17 and IFN-γ expression in CD4$^+$ T cells was analysed by flow cytometry. For the 5-bromo-2′-deoxyuridine (BrdU) incorporation assay, the mice were intraperitoneally injected with BrdU (1 mg per mouse, Sigma-Aldrich) on day 10. Eighteen hours later, CD4$^+$ T cells isolated from the spleen were analysed by flow cytometry using fluorescein isothiocyanate (FITC)-conjugated anti-BrdU (3D4, BD Biosciences).

Animals were scored for clinical signs of EAE for 23 days using the following criteria: 0, no clinical signs; 1, limp tail (tail paralysis); 2, complete loss of tail tonicity or abnormal gait; 3, partial hind limb paralysis; 4, complete hind limb paralysis; 5, forelimb paralysis or moribund; and 6, death. Histological analyses were performed as described[31].

CD4$^+$ T-cell transfer. CD4$^+$ T cells were prepared from the spleens of wild-type and *Nfkbiz*$^{-/-}$ mice using the CD4$^+$ T Cell Isolation Kit (Miltenyi Biotec) (purity was >95%). CD4$^+$ T cells (7×10^6 per mouse) were injected intravenously into *Rag2*$^{-/-}$ mice. One day later, the recipient mice were subjected to EAE induction.

Purification of dendritic cells and dendritic cell–T cell co-culture. PDCA1$^+$ cells and PDCA1$^-$CD11c$^+$ cells were used as plasmacytoid and conventional dendritic cells, respectively, which were isolated from the spleen using anti-PDCA1 microbeads and anti-CD11c microbeads (Miltenyi Biotec) (purity was >95%). In the presence of either 100 ng ml^{-1} lipopolysaccharide (LPS; Sigma-Aldrich) or 100 nM endotoxin-free phosphorothioate-stabilized CpG oligodeoxynucleotides (5′-TCCATGACGTTCCTGATGCT-3′) (Hokkaido System Science), naive CD4$^+$ T cells were co-cultured with dendritic cells in the presence of 1 ng ml^{-1} soluble anti-CD3, 2.5 ng ml^{-1} TGF-β, 10 μg ml^{-1} anti-IFN-γ and 10 μg ml^{-1} anti-IL-4. Three days later, cells were restimulated with 40 ng ml^{-1} PMA plus 0.5 μg ml^{-1} ionomycin in the presence of GolgiPlug for 4 h, after which CD4$^+$ T cells were analysed for intracellular IL-17 and IFN-γ. For analysis of cytokine production and surface marker expression, dendritic cells were cultured with 100 ng ml^{-1} LPS or 100 nM CpG DNA for 24 h.

Quantitative RT–PCR. Total RNA was extracted with ISOGEN (Wako). Quantitative RT–PCR was performed with a LightCycler (Roche) using SYBR Green (Toyobo) as described[31]. The primer sequences are described in Supplementary Table 1. The level of mRNA expression was normalized to that of *Gapdh* mRNA expression.

ELISA. Concentrations of cytokines in the culture supernatant were determined by ELISA kits (IFN-γ, IL-4 and IL-17, BD Biosciences; IL-6 and TNF-α, eBioscience), according to the manufacturers' instructions.

Retroviral transduction. pMX-IRES-EGFP and pMX-IRES-hCD2 are bicistronic retroviral vectors containing enhanced green fluorescence protein (EGFP) and human CD2 lacking the cytoplasmic domain, respectively, under the control of an internal ribosome entry site (IRES)[32]. The cDNA fragments of CD2, RORγt, RORα, RelA, cRel and p50 were amplified by PCR. cDNA fragments of IκBζ splicing variants and truncated mutants[19] were cloned into pMX-IRES-EGFP or pMX-IRES-hCD2 with a Myc tag added at its 5′ end. cDNA fragments of RORγt, RORα, RelA, cRel and p50 were cloned into pMX-IRES-EGFP. Retroviral packaging was performed by transfecting Plat-E cells with the plasmids as described previously[33]. Naive CD4$^+$ T cells were plated in wells pre-coated with 100 μg ml^{-1} goat anti-hamster IgG (Cappel) followed by 0.5 μg ml^{-1} anti-CD3 and 0.5 μg ml^{-1} anti-CD28 for 3 days in the presence of 5 ng ml^{-1} IL-2 (PeproTech) under the following conditions: anti-IL-4, anti-IFN-γ for T_H0 (neutral conditions); anti-IL-4, anti-IFN-γ, IL-6 and TGF-β for T_H17. In Supplementary Fig. 14, 10 μg ml^{-1} anti-TGF-β (1D11, R&D Systems) were added into the cultures. On days 1 and 2, cells were infected with fresh retroviral supernatant by centrifugation for 2 h at 780*g* in the presence of 10 μg ml^{-1} polybrene (Sigma-Aldrich). Cells were further cultured for 3 days. For intracellular cytokine staining, cells were restimulated for 4 h with 40 ng ml^{-1} PMA plus 0.5 μg ml^{-1} ionomycin in the presence of GolgiPlug. For quantitative RT–PCR and immunoblot analyses, EGFP$^+$ cells were sorted by MoFlo (Beckman Coulter).

Flow cytometry and antibodies. For the analysis of natural T_{reg} cells, single-cell suspensions prepared from the thymus, spleen and lymph nodes were stained with fluorophore-conjugated monoclonal antibodies: FITC-conjugated anti-CD4 (RM4-5, BD Biosciences), phycoerythrin-cyanine 7-conjugated anti-CD25 (PC61, BD Biosciences) and allophycocyanin-conjugated anti-Foxp3 (FJK-16 s, eBioscience). For intracellular cytokine staining, phycoerythrin-conjugated anti-mouse IL-17 (TC11-18H10, BD Biosciences), allophycocyanin-conjugated anti-mouse IFN-γ (XMG1.2, BD Biosciences) and allophycocyanin-conjugated anti-human CD2 (LFA-2, eBioscience) were used. For the analysis of the phosphorylation of STAT3, cells were stained with anti-phospho-STAT3 (D3A7, Cell Signaling Technology) followed by FITC-conjugated goat anti-rabbit IgG (BioSource). Flow cytometric analysis was performed by FACSCanto II with Diva software (BD Biosciences).

Reporter gene assay. The reporter plasmid Il17-Luc, Il17 4371-Luc and Il17 1547-Luc were constructed by subcloning a 6,647-base-pair (bp) fragment, a 4,371-bp fragment and a 1,547-bp fragment of the 5′ flanking region of the mouse *Il17a* gene, respectively, into the pGL3-basic vector (Promega). Il17 CNS2-Luc was constructed by subcloning the CNS2 region of the *Il17a* gene into the pTAL-Luc (Clontech). The mutations introduced into Il17 CNS2-Luc were as follows: 5′-AGGGACTGTCCC-3′ (ISE1) to 5′-AAATACTGTCCC-3′; 5′-GGGAAAA CACT-3′ (ISE2) to 5′-AATAAAACACT-3′; 5′-GGAAGCGCCT-3′ (ISE3) to 5′-ATAAGCGCCT-3′. The expression plasmids of IκBζ (L), (S) and (D) have been described[19]. cDNA fragments of RORγt and RORα amplified by PCR were subcloned into the expression vector. The reporter plasmids and the expression plasmids were transfected into HEK293T cells using FuGENE 6 (Roche). After 36 h, dual luciferase assay was performed according to the manufacturer's protocol (Promega).

Immunoblot analysis. Immunoblot analysis was performed using antibodies against β-actin (Sigma-Aldrich), Myc (MBL) or IκBζ (C-15, Santa Cruz) as described[31].

Chromatin immunoprecipitation assay. Naive CD4$^+$ T cells were activated with plate-bound 2 μg ml^{-1} anti-CD3 and 2 μg ml^{-1} anti-CD28 for 3 days in the presence of anti-IL-4 and anti-IFN-γ for the development of T_H0, or anti-IL-4, anti-IFN-γ, IL-6, TGF-β and IL-23 for the development of T_H17. ChIP assay was performed using antibodies against IκBζ (C-15, Santa Cruz) and normal goat IgG (Santa Cruz) as described with minor modifications[34]. Quantitative PCR was performed with a LightCycler using the primers described in Supplementary Table 2. The data are presented as the relative binding based on normalization to input DNA. The evolutionarily conserved regions were identified as regions sharing at least 70% sequence identity across at least 100 bp using the rVista 2.0 web tool[35].

Statistical analysis. All data are expressed as the mean ± s.e.m. ($n = 3$ or more). Statistical analysis was performed using the unpaired two-tailed Student's *t*-test

($*P < 0.05$; $**P < 0.01$; $***P < 0.005$; NS, not significant, throughout the paper). Results are representative examples of more than three independent experiments.

25. Kurebayashi, S. *et al.* Retinoid-related orphan receptorγ (RORγ) is essential for lymphoid organogenesis and controls apoptosis during thymopoiesis. *Proc. Natl Acad. Sci. USA* **97,** 10132–10137 (2000).
26. Adachi, O. *et al.* Targeted disruption of the MyD88 gene results in loss of IL-1- and IL-18-mediated function. *Immunity* **9,** 143–150 (1998).
27. Nakae, S. *et al.* Antigen-specific T cell sensitization is impaired in IL-17-deficient mice, causing suppression of allergic cellular and humoral responses. *Immunity* **17,** 375–387 (2002).
28. Sha, W. C., Liou, H. C., Tuomanen, E. I. & Baltimore, D. Targeted disruption of the p50 subunit of NF-κB leads to multifocal defects in immune responses. *Cell* **80,** 321–330 (1995).
29. Hamilton, B. A. *et al.* Disruption of the nuclear hormone receptor RORα in *staggerer* mice. *Nature* **379,** 736–739 (1996).
30. Takeda, K. *et al.* Stat3 activation is responsible for IL-6-dependent T cell proliferation through preventing apoptosis: generation and characterization of T cell-specific Stat3-deficient mice. *J. Immunol.* **161,** 4652–4660 (1998).
31. Asagiri, M. *et al.* Cathepsin K-dependent toll-like receptor 9 signaling revealed in experimental arthritis. *Science* **319,** 624–627 (2008).
32. Kitamura, T. *et al.* Retrovirus-mediated gene transfer and expression cloning: powerful tools in functional genomics. *Exp. Hematol.* **31,** 1007–1014 (2003).
33. Shinohara, M. *et al.* Tyrosine kinases Btk and Tec regulate osteoclast differentiation by linking RANK and ITAM signals. *Cell* **132,** 794–806 (2008).
34. Koga, T. *et al.* NFAT and Osterix cooperatively regulate bone formation. *Nature Med.* **11,** 880–885 (2005).
35. Loots, G. G. & Ovcharenko, I. rVISTA 2.0: evolutionary analysis of transcription factor binding sites. *Nucleic Acids Res.* **32,** W217–W221 (2004).

Unique multipotent cells in adult human mesenchymal cell populations

Yasumasa Kuroda[a,1], Masaaki Kitada[a,1], Shohei Wakao[a], Kouki Nishikawa[b], Yukihiro Tanimura[a], Hideki Makinoshima[a], Makoto Goda[c], Hideo Akashi[a], Ayumu Inutsuka[b], Akira Niwa[d], Taeko Shigemoto[a], Yoko Nabeshima[e], Tatsutoshi Nakahata[d], Yo-ichi Nabeshima[e], Yoshinori Fujiyoshi[b], and Mari Dezawa[a,2]

[a]Department of Stem Cell Biology and Histology, Graduate School of Medicine, Tohoku University, Sendai 980-8575, Japan; [b]Department of Biophysics, Graduate School of Science, Kyoto University, Kyoto 606-8502, Kyoto, Japan; [d]Center for iPS Cell Research and Application, Kyoto University, Kyoto 606-8507, Japan; [e]Department of Pathology and Tumor Biology, Graduate School of Medicine, Kyoto University, Kyoto 606-8501, Japan; and [c]Japan Biological Informatics Consortium (Kyoto Branch Office), Oiwake, Kitashirakawa, Sakyo-ku, Kyoto 606-8502, Japan

Edited* by Yoshito Kaziro, Kyoto University, School of Medicine, Kyoto, Japan, and approved March 29, 2010 (received for review October 8, 2009)

We found adult human stem cells that can generate, from a single cell, cells with the characteristics of the three germ layers. The cells are stress-tolerant and can be isolated from cultured skin fibroblasts or bone marrow stromal cells, or directly from bone marrow aspirates. These cells can self-renew; form characteristic cell clusters in suspension culture that express a set of genes associated with pluripotency; and can differentiate into endodermal, ectodermal, and mesodermal cells both in vitro and in vivo. When transplanted into immunodeficient mice by local or i.v. injection, the cells integrated into damaged skin, muscle, or liver and differentiated into cytokeratin 14-, dystrophin-, or albumin-positive cells in the respective tissues. Furthermore, they can be efficiently isolated as SSEA-3(+) cells. Unlike authentic ES cells, their proliferation activity is not very high and they do not form teratomas in immunodeficient mouse testes. Thus, nontumorigenic stem cells with the ability to generate the multiple cell types of the three germ layers can be obtained through easily accessible adult human mesenchymal cells without introducing exogenous genes. These unique cells will be beneficial for cell-based therapy and biomedical research.

bone marrow | differentiation | fibroblasts | mesenchymal stem cell | pluripotency

Recent advances in stem cell research have revealed the existence of various types of tissue stem cells that contribute to the functional maintenance of organs and to cell renewal, tissue remodeling, and repair (1, 2). These stem cells are expected to contribute to regenerative medicine, but this will require elucidation of their stem cell properties to control their proliferation and differentiation. Among the many kinds of tissue stem cells, hematopoietic stem cells and neural stem cells have been characterized most extensively (i.e., their ability to self-renew and differentiate into tissue-specific cell types has been clearly demonstrated at the single-cell level) (3, 4). In contrast, some of the properties of mesenchymal stem cells remain obscure. For example, one mesenchymal cell type, the bone marrow stromal cell (MSC), differentiates into cells of the same mesenchymal lineage, such as osteocytes, cartilage, and adipocytes, but also differentiates into cells of other lineages, such as neuronal cells and liver cells, suggesting that their differentiation is not tissue-specific, and that they are thus qualified as multipotent cells (5–8). In most cases, however, the differentiation was demonstrated in a heterogeneous population comprising MSCs and not at the single-cell level. Therefore, it remains under debate whether different subsets of cells are responsible for differentiation into cell types of different lineages, such as osteocytes and neuronal cells, or whether a distinctly multipotent stem cell type exists that is responsible for differentiation across all the oligo-lineage boundaries. Furthermore, hair follicle stem cells and dermal stem cells of the skin differentiate into cells positive for neuronal and smooth muscle cell markers, but their differentiation into cells of all three germ layers has not been demonstrated at the single-cell level (9–11).

In the present study, we demonstrate, at the single-cell level, that adult human skin fibroblasts, MSCs, and native bone marrow aspirates contain a distinct type of stem cell that is capable of generating cells with characteristics of all three germ layers. These cells are indistinguishable from other major mesenchymal cells in adherent culture, but when they are transferred to suspension culture, they form characteristic cell clusters that are positive for pluripotency markers and exhibit self-renewal and differentiation. Furthermore, they can be efficiently isolated as cells positive for both SSEA-3, a human pluripotency marker, and CD105, a mesenchymal cell marker. The cells exhibit multipotency, but their proliferation activity is not very high. Furthermore, although retaining their differentiation ability in vivo, these cells, unlike authentic ES cells, do not form teratomas in testes of immunodeficient mice. Our findings thus suggest that adult human mesenchymal cell populations, such as skin fibroblasts and MSCs, contain distinctly multipotent stem cells and that further studies of these cells will promote a better understanding of mesenchymal stem cell properties. Collection and enrichment of these cells should contribute to improved differentiation efficiency in mesenchymal cell populations. Finally, because these cells are easily accessible, they will be a realistic source of adult human multipotent stem cells that are capable of differentiation into cells with characteristics of all three germ layers without the need to introduce exogenous genes. These cells thus hold great promise for cell-based therapy and biomedical research.

Results

Analysis of Cell Clusters Generated from Human Mesenchymal Cells. We found that naive human MSCs (H-MSCs) grown in adherent culture spontaneously formed characteristic cell clusters at a very low frequency that appeared similar to clusters formed by human ES cells at an early stage (Fig. 1*A*) (12), suggesting that naive H-MSCs might contain multipotent cells. At a certain size, these cell clusters stopped growing and had a heterogeneous appearance (Fig.1*B*).

Dormant tissue stem cells are activated when tissues are exposed to stress, burdens, or damage (13–16). We therefore explored the possibility of whether stress conditions could be exploited for a method to enrich the putative stem cells in adult human mesenchymal cell populations. We subjected two strains of human skin fibroblasts (H-fibroblasts) and four strains of H-MSCs to six

Author contributions: M.D. designed research; Y.K., M.K., S.W., K.N., Y.T., H.M., M.G., H.A., A.I., A.N., T.S., Y.N., T.N., Y.F., and M.D. performed research; Y.K., M.K., S.W., T.N., Y.-i.N., Y.F., and M.D. analyzed data; and M.K., Y.F., and M.D. wrote the paper.

The authors declare no conflict of interest.

*This Direct Submission article had a prearranged editor.

[1]Y.K. and M.K. contributed equally to this work.

[2]To whom correspondence should be addressed. E-mail: mdezawa@m.tains.tohoku.ac.jp.

This article contains supporting information online at www.pnas.org/lookup/suppl/doi:10.1073/pnas.0911647107/-/DCSupplemental.

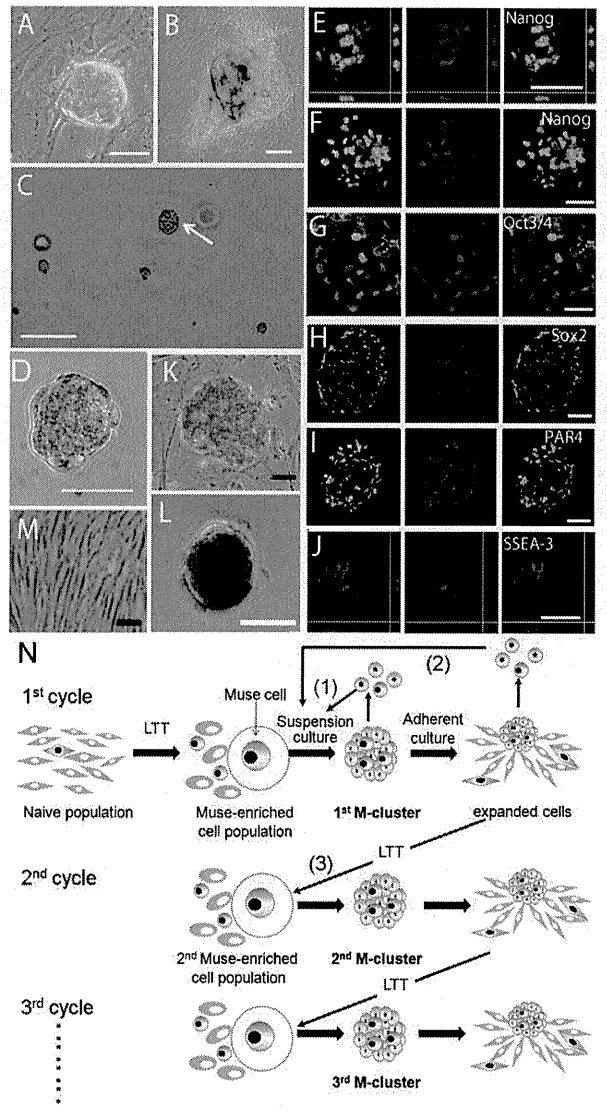

Fig. 1. Characterization of M-clusters. (*A* and *B*) Characteristic cell clusters that occur spontaneously in adherent cultures of naive H-MSCs. (*C* and *D*) MC culture of H-fibroblasts on day 7 showing an M-cluster (*C*, arrow). Immunocytochemical localization of Nanog (*E* and *F*), Oct3/4 (*G*), Sox2 (*H*), PAR4 (*I*), and SSEA-3 (*J*) in M-clusters formed by H-fibroblasts (*E*, *I*, and *J*) and H-MSCs (*F*, *G*, and *H*). ALP(+) human ES cells (*K*), M-cluster (H-fibroblast) (*L*), and naive H-fibroblasts (*M*). (*N*) Schematic diagram of the self-renewal of Muse cells. (Scale bars: *A*–*C*, 100 μm; *D*–*M*, 50 μm.)

different stress conditions, including long-term trypsin incubation (LTT) for 8 or 16 hr (Table S1 and *SI Materials and Methods*).

Stem cells are often grown in suspension culture, which is an efficient and convenient method to maintain their stem cell properties (17, 18). H-fibroblasts or H-MSCs that survived the stress treatments were therefore suspended in methylcellulose (MC) medium (19) at a density of 8,000 cells per milliliter (MC culture; *SI Materials and Methods*) and grown for 7 days (Fig. 1*C*). Each condition gave rise to cell clusters with sizes of up to 50–150 μm in diameter (Fig. 1*D*). Using different filters, we separated the cell clusters according to their size and characterized them by immunocytochemistry. Most of the clusters with a diameter larger than 25 μm contained cells positive for the pluripotency markers Nanog, Oct3/4, SSEA-3, PAR-4, and Sox2 and were positive for alkaline phosphatase (ALP) staining (Fig. S1). We therefore only counted cell clusters larger than 25 μm. Among the stress conditions tested, 16-hr LTT was most potent in the formation of cell clusters in H-fibroblasts, and 8-hr LTT was most potent in the formation of cell clusters in H-MSCs (Table S1 and *SI Results*). As expected, the formed clusters contained cells positive for the above pluripotency markers (Fig. 1 *E*–*J*) and ALP staining (Fig. 1 *K*–*M*). We called these cells multilineage differentiating stress enduring (Muse) cells because they express pluripotency markers; as described below, they differentiate into ectodermal, endodermal, and mesodermal cells; and they endure through stress conditions. We refer to H-fibroblasts and H-MSCs treated with 16-hr and 8-hr LTT, respectively, as "Muse-enriched cell populations" (MEC populations).

To calculate the frequency of Muse-cell-derived cell cluster (M-cluster; *SI Results*) formation accurately, MEC populations derived from both H-fibroblasts and H-MSCs were subjected to single-cell suspension culture after limiting dilution (Fig. S2 and *SI Materials and Methods*), showing that 11.6 ± 1.6% of the cells in the H-fibroblast–MEC population and 8.1 ± 0.2% of the cells in the H-MSC–MEC population proceeded to form M-clusters after 7 days. Naive populations (without LTT) were also examined and showed that 1.3 ± 0.1% (H-fibroblasts) and 1.1 ± 0.1% (H-MSCs) of the cells formed M-clusters in single-cell suspension culture after limiting dilution.

Self-Renewal and Expansion of Muse Cells. After LTT, Muse cells began to divide after 1–2 days in MC culture and continued to divide at a rate of ≈1.3 days per cell division until day 8, forming cell clusters. Cell proliferation gradually slowed by days 11–12 and ceased around day 14, with cell clusters reaching a maximum size of 150 μm (Fig. S3 and *SI Materials and Methods*).

When M-clusters formed in single-cell suspension culture after limiting dilution (day 12) were dissociated into single cells by a 5-min trypsin treatment and returned to single-cell suspension culture, the cells survived but divided very slowly (5–7 days per cell division) or sometimes not at all (Fig. 1*N1*). However, transfer of single M-clusters to adherent culture reinitiated cell proliferation and produced expanded cells. When cultures that had expanded to ≈3,000–5,000 cells were dissociated and subjected to single-cell suspension culture without LTT, 48.0 ± 5.8% (H-fibroblasts) and 40.3 ± 9.1% (H-MSCs) of the cells formed M-clusters (Fig. 1*N2*). When cultures were allowed to expand to $5–10 \times 10^4$ cells and were then subjected to LTT to produce MEC populations (Fig. 1*N3*), 12.3 ± 1.3% (H-fibroblasts) and 8.5 ± 0.5% (H-MSCs) of these cells formed second generation M-clusters. We repeated this culture cycle, consisting of LTT → suspension culture → adherent culture, five times, and every cell generation showed similar behavior and a similar frequency of M-cluster formation. We also confirmed that the fifth generation M-clusters were still positive for pluripotency markers and ALP staining. Furthermore, karyotypes of cells expanded from M-clusters did not show detectable abnormalities (Fig. S4 and *SI Results*). In conclusion, the proliferation activity of Muse cells is not very high, and proliferation stops in suspension culture when the cell clusters reach a defined size. Nevertheless, the proliferation of Muse cells can be reinitiated by transfer to adherent culture, which is followed by the formation of next-generation M-clusters, demonstrating the capacity of Muse cells for self-renewal and proliferation.

Differentiation of M-Clusters. To analyze their differentiation ability, single M-clusters formed in single-cell suspension culture after limiting dilution were transferred onto gelatin-coated dishes. After 7 days of culture, immunocytochemistry revealed cells positive for neurofilament-M [an ectodermal marker; the ratio of positive cells was 3.5 ± 0.5% (H-fibroblasts) and 3.7 ± 0.6% (H-MSCs)], α-smooth muscle actin [α-SMA; mesodermal, 12.2 ± 1.8% (H-fibroblasts) and 8.0 ± 0.6% (H-MSCs)], α-fetoprotein [endodermal, 2.7 ± 0.1% (H-fibroblasts) and 3.2 ± 0.3% (H-MSCs)], cytokeratin 7 [endodermal, 5.5 ± 0.1% (H-fibroblasts) and 3.4 ± 0.6% (H-MSCs)], or desmin [mesodermal, 14.2 ± 0.4% (H-fibroblasts) and 10.1 ± 0.5% (H-MSCs)] (Fig. 2*A*–*E*). RT-PCR of cells derived from first- and third-generation M-clusters confirmed that these cells

expressed α-fetoprotein (endodermal) and GATA6 (endodermal), microtubule-associated protein-2 (MAP-2; ectodermal), and Nkx2.5 (mesodermal), whereas these markers were not clearly detected in naive fibroblasts and MSC populations (Fig. 2*F*).

We injected MEC populations or M-clusters into the testes of immunodeficient mice to test whether they form teratomas. None of the testes injected with MEC populations or M-clusters formed teratomas for up to 6 months, and most of the testes were not significantly larger than control testes (Fig. 2*G* and *SI Results*). In the MEC- or M-cluster-injected testes, cells positive for human mitochondria and for ectodermal (neurofilament), endodermal (α-fetoprotein), and mesodermal (SMA) lineage markers were detected (Fig. 2 *H–M* and Fig. S5).

We next tested the differentiation of MEC populations in vivo by transplanting the cells into damaged tissues of the back skin (by local injection of GFP-labeled H-MSC–MEC population), gastrocnemius muscle (i.v. injection of GFP-H-fibroblast–MEC population), or liver (i.v. injection of GFP-H-fibroblast–MEC population) of immunodeficient mice. In regenerating skin, after 2 weeks, 79.5 ± 2.0% of the transplanted cells in the epidermis also expressed cytokeratin 14 (Fig. 3*A*). GFP(+) cells were also incorporated into regenerating muscle. After 2 weeks, the nuclei of these cells were centrally located, but after 4 weeks, 96.1 ± 2.2% of the GFP(+) cells had the appearance of mature myofibers with peripheral nuclei and expressed human dystrophin (Fig. 3 *B* and *C*). Some of the transplanted cells expressed satellite cell marker Pax7 (Fig. 3*B*). In the regenerating liver, after 4 weeks, most of the cells positive for human Golgi complex expressed human albumin (84.9 ± 5.3%) and human antitrypsin (87.6 ± 3.0%; Fig. 3 *D* and *E*). These data suggest that MEC populations can differentiate into ectodermal, endodermal, and mesodermal lineage cells in vivo.

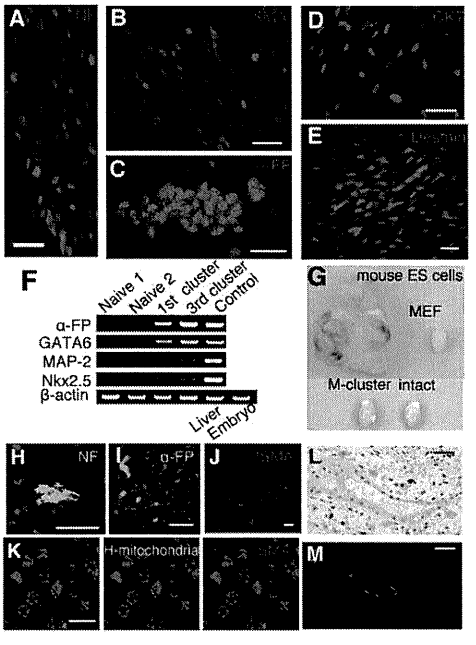

Fig. 2. Differentiation of Muse cells in vitro and in testes. Immunocytochemistry of neurofilament-M (NF) (*A*), α-SMA (*B*), α-fetoprotein (α-FP) (*C*), cytokeratin 7 (CK7) (*D*), and desmin (*E*) in cells derived from a single M-cluster (H-fibroblasts). (*F*) RT-PCR analysis of naive cells and first- and third-generation M-clusters (first and third clusters) derived from H-fibroblasts. Positive controls were human fetus liver (Liver) for α-FP and whole human embryo (Embryo) for GATA6, MAP-2, and Nkx2.5. (*G–M*) Testes of immunodeficient mice injected with cells. (*G*) Uninjected testes (intact) and testes injected with mouse ES cells (8 weeks), mouse embryonic fibroblast (MEF) cells (8 weeks), and M-clusters (6 months). Immunohistochemistry of NF (*H*), α-FP (*I*), and SMA (*J*) in testes injected with MEC populations and M-clusters. (*K*) Double-labeling of human mitochondria (green) and SMA (red). The tube-like structure (*L*) was positive for human mitochondria in the adjacent section (*M*; red). (Scale bars: *A–E* and *H–L*, 50 μm; *M*, 20 μm.)

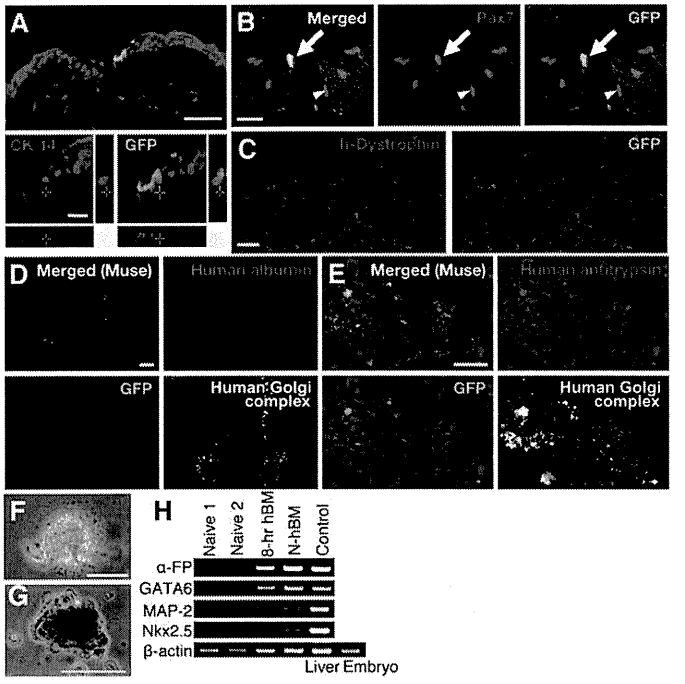

Fig. 3. Transplantation of Muse cells and M-cluster formation from bone marrow. (*A–E*) Differentiation of GFP-labeled MEC population (H-fibroblasts) in damaged tissues of immunodeficient mice. (*A*) Cells locally injected into the edge of the excised region. Transplanted GFP(+) cells expressed cytokeratin 14 (red) in the regenerating epidermis (2 weeks). (*B*) Two weeks after i.v. injection, GFP(+) cells with central nuclei were seen in cardiotoxin-injected cutaneous muscle. Transplanted GFP(+) cells (arrow) and host cells [GFP(–), arrowhead] that expressed Pax7 were seen. (*C*) After 4 weeks, the GFP(+) muscle fibers expressed human dystrophin (h-Dystrophin; red). Four weeks after i.v. injection, most of the transplanted GFP(+) cells in liver with CCl_4-induced damage were positive for human Golgi complex (*D* and *E*, white); some of them expressed human albumin (*D*, red) or human antitrypsin (*E*, red). (*F–H*) Formation of M-clusters from bone marrow-derived mononucleated cells. (*F*) M-clusters formed with 8-hr LTT (8-hr hBM-MC, day 7). (*G*) ALP(+) cells in 8-hr hBM-MC (day 7). (*H*) RT-PCR of naive H-MSCs (Naive 1 and Naive 2); M-clusters formed with 8-hr LTT (8-hr hBM) or without LTT [Naive hBM (N-hBM)]. Positive controls were human fetus liver (Liver) for α-fetoprotein (α-FP) and whole human embryo (Embryo) for GATA6, MAP-2, and Nkx2.5. (Scale bars: *A*, *B*, *E*, *F*, and *G*, 50 μm; *C* and *D*, 100 μm.)

M-Cluster Formation Directly from Native Bone Marrow Aspirate. The experiments described so far were performed with Muse cells and M-clusters derived from cell cultures, which may have acquired characteristics that differ from those of cells in situ. Mesenchymal cells are known to reside in the mononucleated cell fraction of bone marrow, which can be collected directly from native tissue without culturing. We therefore tested whether cells directly collected from human bone marrow (hBM) would also be able to form M-clusters. Isolated mononucleated cells were either subjected directly to MC culture (naive hBM-MC) or to 8-hr LTT before MC culture (8-hr hBM-MC). After 7 days, 8-hr hBM-MC formed M-clusters at a frequency of 0.3 ± 0.04%, ≈60–75 times higher than that of naive hBM-MC (0.004 ± 0.001%) (Fig. 3*F*). M-clusters from both naive hBM-MC and 8-hr hBM-MC were ALP(+) (Fig. 3*G*), and RT-PCR of cells expanded from single M-clusters on gelatin-coated dishes showed expression of α-fetoprotein, GATA6, MAP-2, and Nkx2.5 (Fig. 3*H*). These results suggest that M-clusters can be formed directly from hBM and that they can be enriched by 8-hr LTT.

Naive hBM-MC formed M-clusters at an extremely low frequency. Because culturing can change the composition of cell populations,

DEVELOPMENTAL

cells in stable culture may have a different propensity to form M-clusters than cells from native tissues. To test this possibility, we grew hBM aspirate in adherent culture to collect primary MSCs and subjected the cells directly to MC culture without 8-hr LTT. This protocol resulted in a much higher frequency of M-cluster formation of 0.3 ± 0.08%. When primary MSCs were further cultured to the second and fifth passages, the frequency of M-cluster formation without LTT increased up to 0.5 ± 0.04% and 0.9 ± 0.1%, respectively. Consistent with this finding, 1.3 ± 0.1% of naive H-fibroblasts and 1.1 ± 0.1% of naive H-MSCs formed M-clusters in single-cell suspension culture as described above. These results suggest that Muse cells have a high stress tolerance and can endure in vitro culture and the subculture procedures.

Bone marrow contains many cell types, including MSCs, hematopoietic lineage cells, and endothelial cells (19). To determine which fraction contains the Muse cells, we isolated mononucleated cells from hBM aspirate and subjected them to magnetic affinity cell sorting (MACS) using antibodies against CD34 and CD117 [markers for hematopoietic cells (20)] and CD105 [marker for MSCs (5, 7)]. We then subjected the cells to 8-hr LTT and allowed them to grow in MC culture for 7 days. The $CD34^+/117^+/105^-$ cell fraction produced few M-clusters, but the $CD34^-/117^-/105^+$ fraction produced 50 times more M-clusters than the $CD34^-/117^-/105^-$ fraction (*SI Results*). This result suggests that the majority of Muse cells belong to the CD105(+) mesenchymal cell population.

Characteristic Features of Muse Cells. FACS analysis revealed that among tested surface markers, MEC populations showed a substantially increased number of cells that were SSEA-3(+) [a human pluripotency marker (12)] compared with naive populations (Fig. 4*A* and *SI Results*). The percentage of SSEA-3(+) cells detected by FACS [1.1 ± 0.05% (H-MSCs) and 1.8 ± 0.22% (H-fibroblasts); Fig. 4*A*] and immunocytochemistry [0.7 ± 0.1% (H-fibroblasts); Fig. 4*B*] in naive cells approached the previously determined frequency of M-cluster formation in single-cell suspension culture (≈1%), as described above. For MEC populations, the percentage of SSEA-3(+) cells detected by FACS [11.6 ± 0.15% (H-MSCs) and 8.6 ± 0.0.32% (H-fibroblasts); Fig. 4*A*] was also comparable to the frequency of M-cluster formation in single-cell suspension culture [11.6 ± 1.6% (H-fibroblasts) and 8.1 ± 0.2% (H-MSCs)] as stated. Furthermore, the expression of Oct3/4 and Sox2 in SSEA-3(+) cells was demonstrated in cultured H-fibroblasts using immunocytochemistry (Fig. 4 *D* and *E*). We therefore used FACS to separate SSEA-3(+) and (−) cells from MEC populations of both H-fibroblasts and H-MSCs and subjected each fraction to single-cell suspension culture after limiting dilution. The result showed that 56.5 ± 3.2% (H-MSCs) and 60.0 ± 4.5% (H-fibroblasts) of the SSEA-3(+) cells generated M-clusters, whereas only a few M-clusters developed in the SSEA-3(−) fraction.

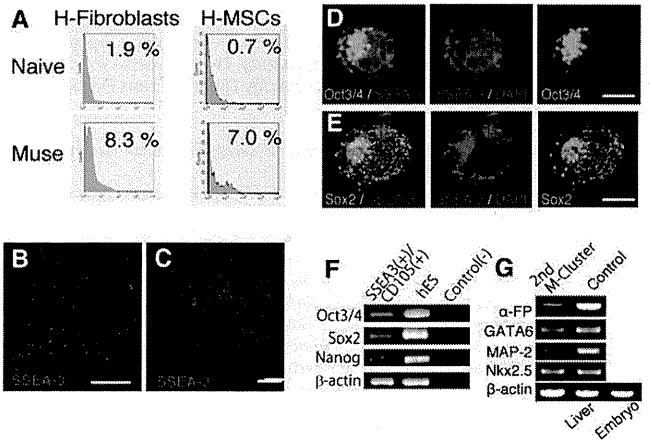

Fig. 4. Characterization of Muse cells. (*A*) FACS analysis for SSEA-3 expression in naive cells (Naive) and MEC populations (Muse) derived from H-fibroblasts and H-MSCs. SSEA-3(+) cells (red) in a naive population (*B*) and in cells expanded from a single M-cluster derived from a FACS-sorted SSEA-3(+) cell (*C*), both from H-fibroblasts. Immunocytochemistry of Oct3/4 (*D*, green, Sox2 (*E*, green), and SSEA-3 (*D* and *E*, red) in Muse cells derived from H-fibroblasts. (*F*) RT-PCR of Oct3/4, Sox2, and Nanog in directly isolated $SSEA\text{-}3^+/CD105^+$ cells from bone marrow, human ES cells for a positive control, and the template without reverse transcription for a negative control [Control(−)]. (*G*) RT-PCR of second-generation M-clusters (2nd M-cluster) from bone marrow-derived mononucleated cells. Positive controls were human fetus liver (Liver) for α-fetoprotein (α-FP) and whole human embryo (Embryo) for GATA6, MAP-2, and Nkx2.5. (Scale bars: *B* and *C*, 100 μm; *D*, 10 μm; *E*–*G*, 5 μm.)

The importance of SSEA-3(+) cells was also seen in the transplantation experiments. In contrast to the integration and differentiation of MEC populations in damaged skin, muscle, and liver (Fig. 3 *A*–*E*), transplantation of SSEA-3(−) populations resulted in a significantly smaller number of integrated cells and fewer cells that were positive for the tissue markers (Fig. S6 and *SI Results*).

Of note, at the scale of 3,000–5,000 cells, only ≈45.0 ± 3.2% (H-fibroblasts) of the cells that expanded from a single FACS-sorted SSEA-3(+) cell were SSEA-3(+) (Fig. 4*C*). This result suggests that proliferation of Muse cells may give rise to Muse cells and non-Muse cells.

The possibility remains that Muse cells are artificially induced by LTT. As described above, the majority of Muse cells exist in the bone marrow's CD105(+) cell fraction. Furthermore, SSEA-3(+) cells showed Muse cell properties. We therefore attempted to collect Muse cells directly from adult hBM aspirates by isolating them as SSEA-3/CD105 double-positive cells. Double-positive cells, which constituted 0.04 ± 0.008% of bone marrow-derived mononucleated cells, were directly subjected to RT-PCR, which showed the expression of Nanog, Oct3/4, and Sox2 in these cells (Fig. 4*F*). Isolated $SSEA\text{-}3^+/CD105^+$ cells were further subjected to single-cell suspension culture after limiting dilution without LTT. At 7 days, 11.4 ± 1.2% of the cells (corresponding to 0.003–0.005% of the mononucleated cells) formed M-clusters that were ALP(+). Single M-clusters were then again expanded in adherent culture to 3,000 cells and subsequently subjected to single-cell suspension culture. Of these cells, 33.5 ± 3.1% formed second-generation M-clusters, and RT-PCR of the cells that expanded from a single M-cluster on gelatin-coated dishes indicated that the cells expressed α-fetoprotein, GATA6, MAP-2, and Nkx2.5 (Fig. 4*G*), suggesting that cells with properties consistent with those of Muse cells reside in adult hBM.

Discussion

We isolated a specific type of human mesenchymal stem cell (i.e., Muse cell) that is capable of generating cells with the characteristics of all three germ layers from a single cell. Muse cells are (*i*) stress tolerant; (*ii*) indistinguishable from general mesenchymal cells in adhesion culture; (*iii*) able to form M-clusters in suspension culture that are positive for pluripotency markers and ALP staining; (*iv*) able to self-renew; (*v*) not very high in their proliferation activity and not shown to form teratomas in immunodeficient mouse testes; (*vi*) able to differentiate into endodermal, ectodermal, and mesodermal cells both in vitro and in vivo; and (*vii*) efficiently isolated from naive tissues as cells positive for both CD105 and SSEA-3.

To investigate whether Muse cells exist in native tissues or whether LTT induces cells to acquire properties of multipotent stem cells, we isolated SSEA-3/CD105 double-positive cells directly from hBM aspirates and subjected them to single-cell suspension culture without LTT. The formation of M-clusters showed that Muse cells or potential Muse cells already exist in adult native hBM. LTT is thus not necessary for collecting Muse cells but is a method to enrich them.

The properties of several kinds of stem cells present in mesenchymal tissue, such as neural crest-derived stem cells (NCSCs) that exist both in the bone marrow and skin, MSCs, skin-derived precursors (SKPs), perivascular cells, and adipose-derived stem

cells, were recently analyzed and described (11, 21–24). Of note, SKPs can be clonally expanded and serve as dermal stem cells for use in skin homeostasis and repair (11). NCSCs can also be clonally expanded, and they may contribute to nerve repair (22). Although, these stem cells can differentiate into ectodermal (e.g., neural marker-positive cells) and mesodermal (e.g., SMA-positive cells, osteocytes, chondrocytes) lineage cells (11, 21–24), their differentiation into representatives of all three germ layers has not been reported. Muse cells are unique among mesenchymal stem cells in that they are able to differentiate not only into ectodermal and mesodermal cells but into endodermal cells. That is, a single Muse cell can generate cells representative of each of the three germ layers. Considering that multilineage differentiation of MSCs, such as into neuronal cells, muscle cells, and liver cells, has been reported (5–8), it is possible that Muse cells contribute to such multilineage differentiation of MSCs.

Muse cells may have practical advantages for regenerative medicine, such as their easy accessibility and differentiation potential. They are not tumorigenic but retain differentiation ability in vivo after transplantation. In fact, they expressed endodermal, ectodermal, and mesodermal lineage markers after injection into mouse testes; integrated into damaged skin, muscle, and liver tissue; and differentiated into cells expressing the respective tissue markers cytokeratin 14 (ectodermal), dystrophin (mesodermal), and albumin (endodermal). Moreover, the multipotency of Muse cells does not need to be induced by the introduction of exogenous genes, and they can be isolated from skin and bone marrow, which are accessible from an individual or from a cell bank. Typically, each tissue contains a very small number of stem cells, and like other stem cells, the proportion of Muse cells in bone marrow-derived mononucleated cells is very small. However, large numbers of Muse cells can be obtained from mesenchymal cell populations by simply cycling the cells through a series of culturing steps, namely, Muse-cell selection followed by formation of M-clusters in suspension culture and expansion of the cells in adherent culture.

Muse cells did not show characteristics of tumorigenic proliferation, and, consistently, they did not develop into teratomas in mice testes. It has recently been reported that epiblast stem cells cultured under certain conditions also did not form teratomas in testes, even though they showed pluripotency in vitro (25). This finding suggests that even pluripotent cells do not always show the formation of teratomas in testes. Furthermore, if Muse cells are normally maintained in adult human tissues, such as in skin fibroblasts, their proliferation must be strictly regulated; otherwise, they would easily form tumors in virtually every part of the body.

Questions regarding the origin, location, and physiological roles of Muse cells in fibroblasts and MSCs will require further study.

Materials and Methods

Culture Cells. Two strains of human skin fibroblasts and four strains of H-MSCs were maintained at 37 °C in α-minimum essential medium (α-MEM) containing 10% (vol/vol) FBS and 0.1 mg/mL kanamycin. Mononucleated cells were collected from six hBM aspirates using Lymphoprep Tubes (Axis-Shield PoC AS). For selection of FBS, an H-MSC clone was plated onto a 24-well dish at a density of 1.5×10^4 cells per cm^2. Serum lots (ES cell grade; HyClone) were checked by adding a sample from each lot to a well at a concentration of 10% (vol/vol) in α-MEM and cultured for 1–2 weeks. The serum in the well that showed the highest frequency of spontaneous cell cluster formation, as shown in Fig. 1 *A* and *B*, was chosen for further experiments.

Generation of MEC Populations and M-Clusters. MEC populations were produced by treating cells with LTT (16 hr for H-fibroblasts and 8 hr for H-MSCs), followed by vortexing at 1,800–2,200 rpm for 3 min (MS1 Minishaker, IKA Works, Staufen, Germany) and centrifugation at 740 × *g* for 15 min. To produce M-clusters, individual cells were cultured in MC or in single-cell suspension culture. For MC culture, culture dishes were first coated with polyHEMA (P3932; Sigma) to avoid attachment of cells to the bottom of the dish. MC (MethoCult H4100; StemCell Technologies) was diluted in 20% (vol/vol) FBS in α-MEM to a final concentration of 0.9%. The cell concentration in the semisolid MC medium was adjusted to be 8×10^3 cells per milliliter. Cells and MC were mixed thoroughly by gentle pipetting, and the mixture was transferred to a polyHEMA-coated dish. At this concentration, the cell-to-cell distance was sufficiently large to minimize cell aggregation. For single-cell suspension culture, MEC populations were subjected to a limiting dilution with 10% (vol/vol) FBS in α-MEM and single cells were plated into each well coated with polyHEMA. The frequency of M-cluster formation was calculated from three experiments for each strain, with a minimum of 250 wells per experiment.

Detailed protocols for cell culture, stress conditions, ALP staining, immunocytochemistry, immunohistochemistry, transplantation experiments, RT-PCR, karyotyping, MACS sorting, and FACS analysis are provided in *SI Text*.

ACKNOWLEDGMENTS. We thank Dr. Thomas Walz (Harvard Medical School) for proofreading the manuscript and Dr. Hiroshi Hamada (Osaka University, Japan) for providing antibodies. We thank the late Keiji Takita, Director General of the Japan New Energy and Industrial Technology Development Organization, who passed away during this study. This work was supported by the Japan New Energy and Industrial Technology Development Organization.

1. Verstappen J, Katsaros C, Torensma R, Von den Hoff JW (2009) A functional model for adult stem cells in epithelial tissues. *Wound Repair Regen* 17:296–305.
2. Nandoe Tewarie RS, Hurtado A, Bartels RH, Grotenhuis A, Oudega M (2009) Stem cell-based therapies for spinal cord injury. *J Spinal Cord Med* 32:105–114.
3. Weissman IL, Shizuru JA (2008) The origins of the identification and isolation of hematopoietic stem cells, and their capability to induce donor-specific transplantation tolerance and treat autoimmune diseases. *Blood* 112:3543–3553.
4. Gage FH (2000) Mammalian neural stem cells. *Science* 287:1433–1438.
5. Pittenger MF, et al. (1999) Multilineage potential of adult human mesenchymal stem cells. *Science* 284:143–147.
6. Dezawa M, et al. (2004) Specific induction of neuronal cells from bone marrow stromal cells and application for autologous transplantation. *J Clin Invest* 113: 1701–1710.
7. Dezawa M, et al. (2005) Bone marrow stromal cells generate muscle cells and repair muscle degeneration. *Science* 309:314–317.
8. Pan RL, et al. (2008) Fetal liver-conditioned medium induces hepatic specification from mouse bone marrow mesenchymal stromal cells: A novel strategy for hepatic transdifferentiation. *Cytotherapy* 10:668–675.
9. Yang JH, Shim SW, Lee BY, Lee HT (2009) Skin-derived stem cells in human scar tissues: A novel isolation and proliferation technique and their differentiation potential to neurogenic progenitor cells. *Tissue Engineering Part C Methods*, 10.1089/ten.tec.2009.0275.
10. Kajahn J, et al. (2008) Skin-derived human adult stem cells surprisingly share many features with human pancreatic stem cells. *Eur J Cell Biol* 87:39–46.
11. Biernaskie J, et al. (2009) SKPs derive from hair follicle precursors and exhibit properties of adult dermal stem cells. *Cell Stem Cell* 5:610–623.
12. Thomson JA, et al. (1998) Embryonic stem cell lines derived from human blastocysts. *Science* 282:1145–1147.
13. Montarras D, et al. (2005) Direct isolation of satellite cells for skeletal muscle regeneration. *Science* 309:2064–2067.
14. Zhang RL, et al. (2006) Reduction of the cell cycle length by decreasing G1 phase and cell cycle reentry expand neuronal progenitor cells in the subventricular zone of adult rat after stroke. *J Cereb Blood Flow Metab* 26:857–863.
15. Hong HS, et al. (2009) A new role of substance P as an injury-inducible messenger for mobilization of CD29(+) stromal-like cells. *Nat Med* 15:425–435.
16. Qiu J, et al. (2009) p27Kip1 constrains proliferation of neural progenitor cells in adult brain under homeostatic and ischemic conditions. *Stem Cells* 27:920–927.
17. Reynolds BA, Weiss S (1992) Generation of neurons and astrocytes from isolated cells of the adult mammalian central nervous system. *Science* 255:1707–1710.
18. Kreso A, O'Brien CA (2008) Colon cancer stem cells. *Current Protocols in Stem Cell Biology*, ed Elefanty A (Wiley, New York).
19. Nakahata T, Spicer SS, Cantey JR, Ogawa M (1982) Clonal assay of mouse mast cell colonies in methylcellulose culture. *Blood* 60:352–361.
20. McKinney-Freeman SL, et al. (2009) Surface antigen phenotypes of hematopoietic stem cells from embryos and murine embryonic stem cells. *Blood* 114:268–278.
21. Fernandes KJ, et al. (2004) A dermal niche for multipotent adult skin-derived precursor cells. *Nat Cell Biol* 6:1082–1093.
22. Nagoshi N, et al. (2008) Ontogeny and multipotency of neural crest-derived stem cells in mouse bone marrow, dorsal root ganglia, and whisker pad. *Cell Stem Cell* 2: 392–403.
23. Crisan M, et al. (2008) A perivascular origin for mesenchymal stem cells in multiple human organs. *Cell Stem Cell* 3:301–313.
24. Gimble JM, Katz AJ, Bunnell BA (2007) Adipose-derived stem cells for regenerative medicine. *Circ Res* 100:1249–1260.
25. Chou YF, et al. (2008) The growth factor environment defines distinct pluripotent ground states in novel blastocyst-derived stem cells. *Cell* 135:449–461.

厚生労働科学研究費補助金
難治性疾患克服研究事業

細網異形成症の診断と治療に関する調査研究

平成２２年～２３年度　総合研究報告書

発行日　平成 24 年 3 月 31 日
発行者　野々山　恵章
発行所　厚生労働省難治性疾患克服研究事業
細網異形成症の診断と治療に関する調査研究班
研究代表者　野々山　恵章
〒359-8513
埼玉県所沢市並木３丁目２番地
ＴＥＬ（04）2995-1621
ＦＡＸ（04）2995-5204